Time-varying data-driven modeling of solar active region and time-dependent solar wind background by SIP-CESE MHD Model

Xueshang Feng(冯学尚)
fengx@spaceweather.ac.cn
Ma XiaoPeng and Jiang Chaowei
SIGMA Weather Group, State Key Lab of Space Weather/CSSAR, CAS

中国科学院空间天气学国家重点实验室
http://www.spaceweather.ac.cn

ASTRONUM-2013 - the 8th Annual International Conference on Numerical Modeling of Space Plasma Flows

2013.07.02

In this talk, a time-dependent MHD modeling driven by the time-dependent observed magnetograms is introduced to study the dynamic evolution of both active region and solar wind background with the help of the 3D Solar-Interplanetary (SIP) adaptive mesh refinement (AMR) space-time conservation element and solution element (CESE) MHD model (SIP-AMR-CESE MHD Model).

A) The simulated evolution of the global solar wind ambient from 2008-07-01 to 2008-08-11 is compared with solar observations and solar wind measurements from both Ulysses and spacecraft near the Earth.

B) Using observed vector magnetogram (& a nonlinear force-free field extrapolation) prior to a sigmoid eruption in AR 11283 as the initial condition, we successfully simulate the realistic initiation process of the eruption event, as is confirmed by a remarkable resemblance to the SDO/AIA observations.

I. Solar-*I*nter*P*lanetary AMR *CESE M*odel (SIP-CESE MHD Model)

Feng et al., ApJ, 2007， JGR，2009; Hu et al., 2008, JGR; Feng et al., APJ, 2010, 2011; Sol. Phys. 2012; Zhou and Feng, JGR, 2012,etc

- Grid in the solar corona

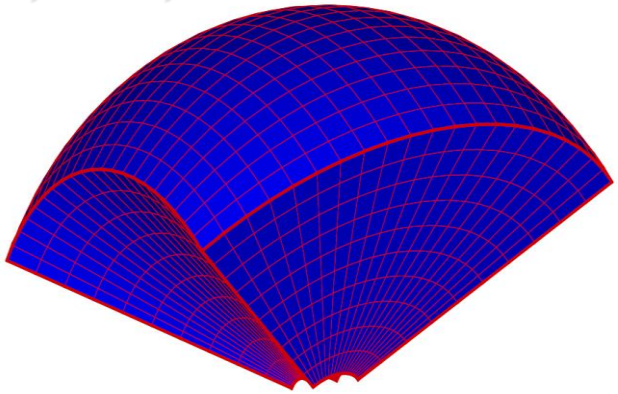

- **Numerical method: Space-Time conservation**

$$\frac{\partial u_m}{\partial t}+\frac{\partial f_m}{\partial x}+\frac{\partial g_m}{\partial y}+\frac{\partial h_m}{\partial z}=\eta_m$$

By Gauss's divergence theorem on space-time conservation cell Vxyzt

$$\oint_{S(V)} \vec{q}_m \cdot d\vec{S} = \int_V \eta_m dV$$

***S*(*V*) is the boundary of a space time region Vxyzt**

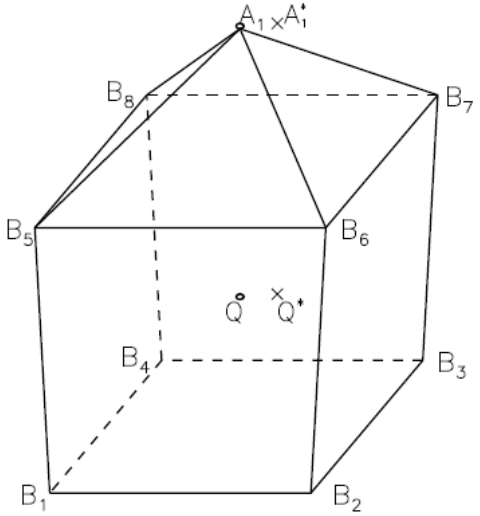

Projection of space-time cell onto space domain

which leads to the implicit solver of nonlinear Newtonian equations.

CESE is different from routine FVM method in that

According to Reynolds transport theorem

$$\frac{\partial}{\partial t}\int_{V_{ijk}} u_m dv + \oint_{S(V_{ijk})} (f_m n_x + g_m n_y + h_m n_z) ds = \int_{V_{ijk}} \eta_m dv$$

$$\int_{V_{ijk}} u_m dv \Big|_{t_1}^{t_2} = \int_{t_1}^{t_2} \left(- \oint_{S(V_{ijk})} (f_m n_x + g_m n_y + h_m n_z) ds + \int_{V_{ijk}} \eta_m dv \right)$$

The rate of change of the total amount of a substance contained in a fixed spatial control volume Vijk is equal to the combination of the two factors: (i) the flux of that substance across the boundary S(Vijk) of the control volume Vijk, and (ii) the integration of the source term over the fixed spatial domain.

$$\frac{d\mathbf{U}_{i,j,k}}{dt} = -\frac{1}{V_{i,j,k}} \sum_{m=1}^{N_f} \left(\vec{\mathbf{F}} \cdot \vec{n}\, \Delta A \right)_{i,j,k,m} + \bar{\mathbf{S}}_{i,j,k} + \bar{\mathbf{Q}}_{i,j,k} = \mathbf{R}_{i,j,k}(\mathbf{U}) ,$$

The conventional finite volume methods concentrate on the evaluation of the right side. Time integration is usually obtained with Runge-Kutta.

OURS is the space-time 4D volume integration

$$\oint_{S(V)} \vec{q}_m \cdot d\vec{S} = \int_V \eta_m dV$$

DII: Grid System from the Sun to Earth space (Feng et al., APJ, 2010; 2011， Solar Physics， 2012)

One component grid in the solar corona

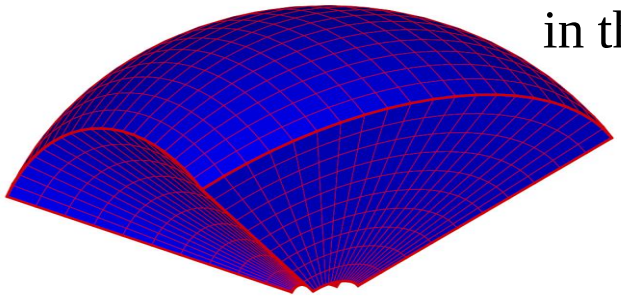

The advantages of this grid system are removal of polar singularities and easy parallel of the (theta,phi) directions

Six-component Grid

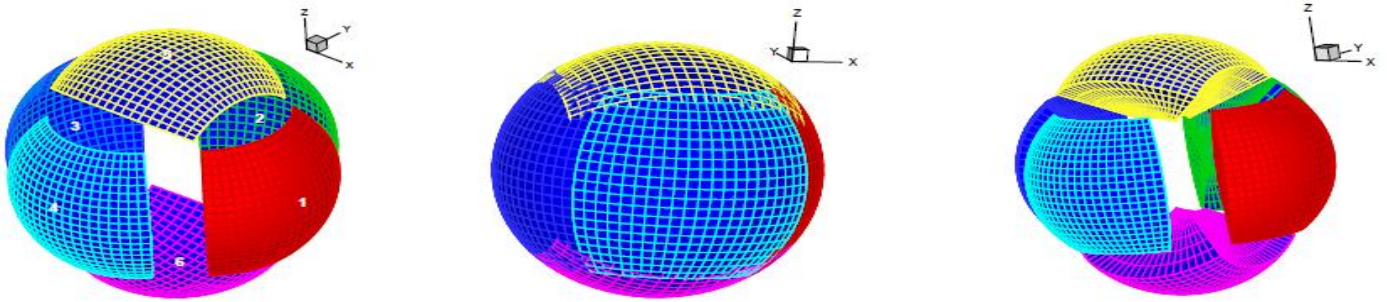

Yin-Yang Grid

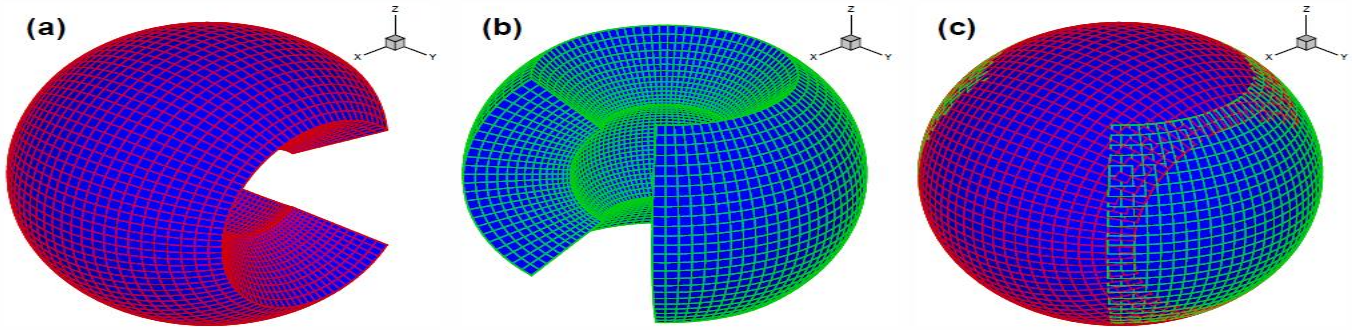

Feng et al., ApJ, 2007， JGR，2009; Hu et al., 2008, JGR; Feng et al., APJ, 2010, 2011; Sol. Phys. 2012; Zhou and Feng, JGR, 2012

DII: AMR Polyhedron Grid—two methods with PARAMESH

Modified by some flux conservation.

I) Coordinate transform (Feng et al., Solar Physics, 2012)

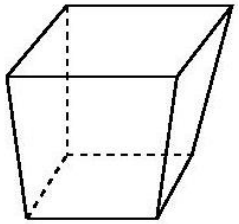

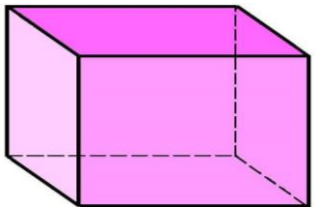

Refinement criterion of the curl of magnetic field

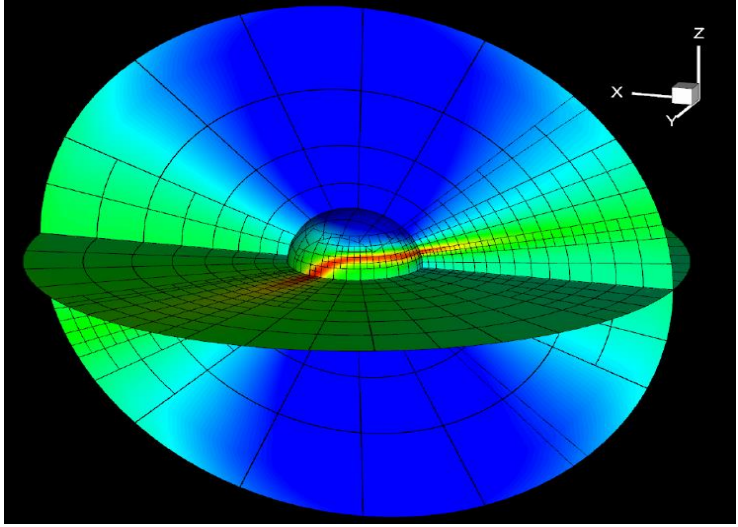

II) Direct AMR by the following orientation

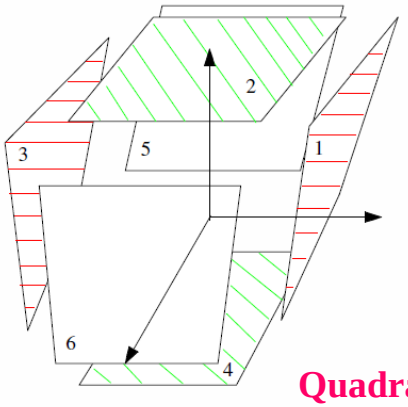

(a)

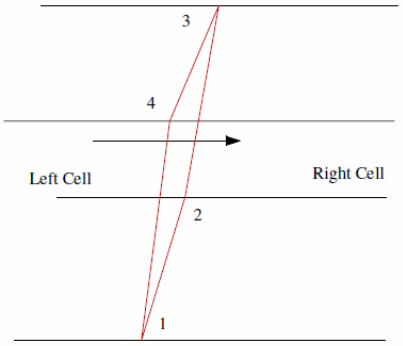

(b)

Quadrangular frustum pyramid

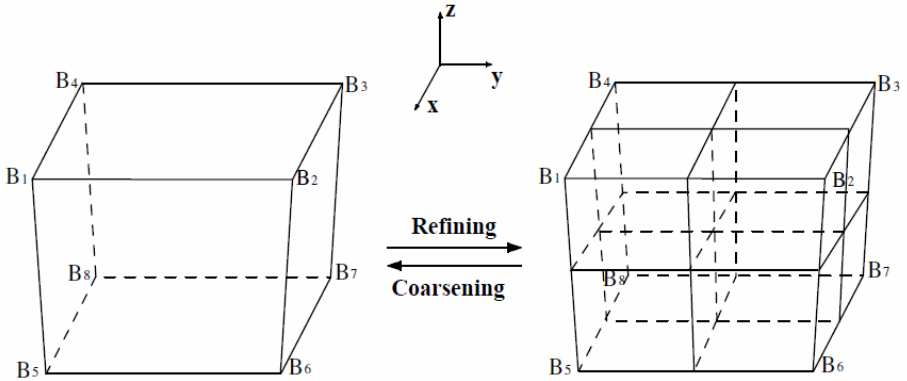

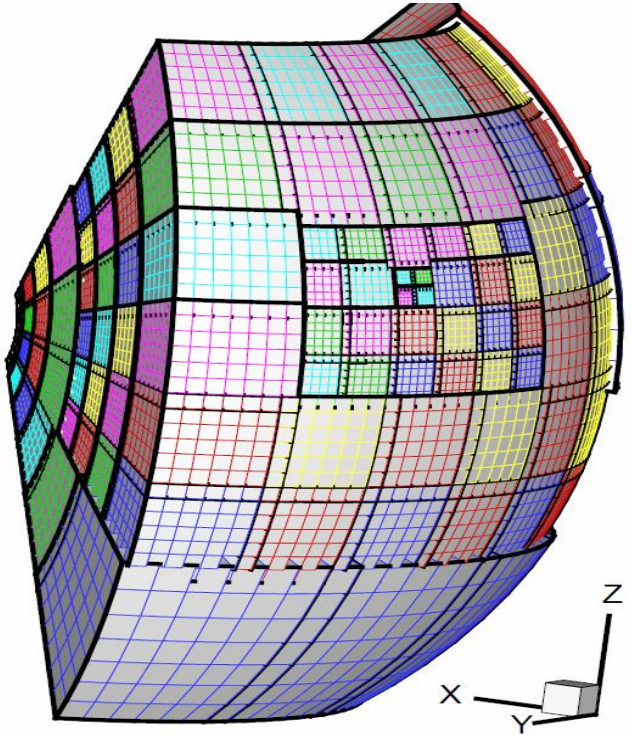

Berger–Oliger algorithm can be applied directly

DIV: Other merits includes

➡ **Div(B) Error Cleaning Method by Fast AMR multigrid Poisson solver (Ricker, ApJS 176:293, 2008）**

➡ **Positivity consideration**

A negative pressure or thermal energy $e = p/(\gamma - 1)$ in the low-β or high speed regions (i.e., $e \ll E$) usually occurs. In such unsafe regions, instead of total energy equation we entropy equation $\frac{\partial e}{\partial t} + \nabla \cdot (eV) = -p\nabla \cdot V + Q_e$ for plasma *β or e/E being very small.*

If negative values still occur, we identify all cells (within the same grid block) that represent physical states surrounding a faulty cell in a rectangular zone up to n_{pos} cells away; and (2) for all but the magnetic field components, replace the faulty cell values by the average of surrounding physical state cells.

➡ **Heating/acceleration by empirically specifying the energy and momentum source heating term with the magnetic field expansion factor fS and the minimum angular separation θb (at the photosphere) between an open field foot point and its nearest coronal hole boundary.**

$$Q_\varepsilon = Q_1 C_a \exp(-\frac{r}{L_{Q1}}) + Q_2 C_a (\frac{r}{Rs} - 1)\exp(-\frac{r}{L_{Q2}}) + \nabla(\xi T^{5/2} \frac{\nabla T \cdot B}{B^2}) \cdot \mathrm{B}$$

$$S_m = M_0 C_a \, (\frac{r}{Rs} - 1)\exp(-\frac{r}{L_M})$$

Wang-Sheeley model

$$C_a = Ca'/\mathrm{Max}(Ca') \text{ with } Ca' = \frac{1}{(1+f_S)^{2/7}} (5.8 - 1.6 \exp[1 - \left(\frac{\theta_b}{8.5}\right)^3])^{3.5}$$

DV: Time-dependent projected characteristic boundary condition is used at the subsonic region by limiting the mass flux escaping through the solar surface with Ulysses observations (e.g., Wu et al., ApJ, 2001; 2006; Hayashi APJ, 2005),

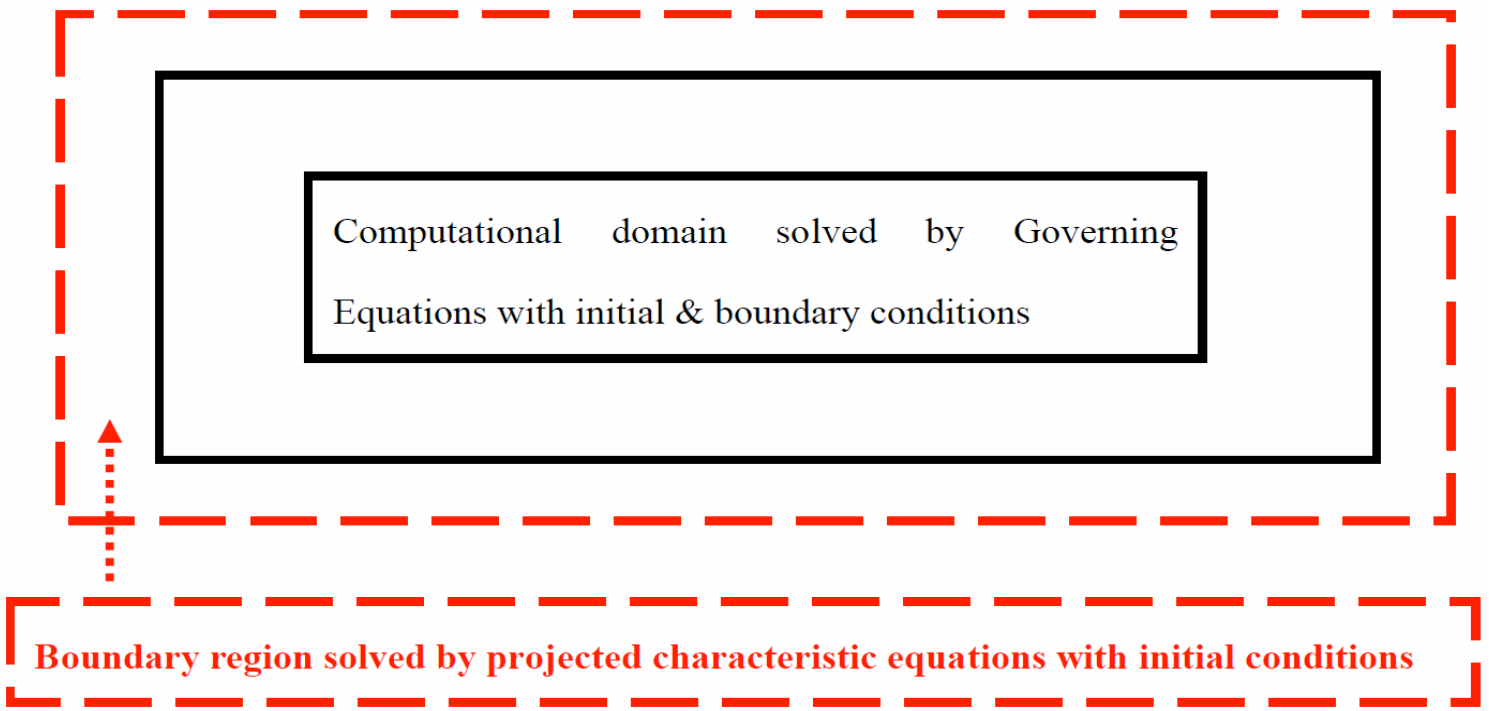

The projected characteristics method **(Wang Hu, Wu, 1982; Wu et al. 2001, Hayashi, ApJS, 2005,Feng et al., ApJ, 2010; 2011;Solar Physics,2011)** is used to couple the surface flux transport (SFT) or time-dependent interpolation change or vector magnetogram with MHD models.

The compatibility equation must be used when updating the boundary variables if the corresponding eigenvalue is negative ($\lambda m < 0$, *i.e.*, the outgoing wave). While for the incoming waves ($\lambda m > 0$), since no observation is available to describe them, we just fix them.

II. Data-driven Solar Wind Model: From 1Rs to 1AU

Background & Motivation:

Global estimates of the solar photospheric magnetic field distribution are critical for space weather forecasting. These global maps are the essential data input for accurate modeling of the corona and solar wind, which is vital for gaining the basic understanding necessary to improve forecasting models needed for really realistic operations. We are now testing the global photospheric field maps generated by the solar surface flux Transport (SFT) model for long-interval synoptic data products **or Time Interpolation** for short-interval synoptic data products **as input to the CESE-MHD coronal and solar wind model.**

Result: Improved, high quality "snapshots" of the Sun's global magnetic field as the input to drive our 3D numerical global coronal AMR-CESE-MHD model

Here, we obtain snapshot of magnetic maps as input to drive our MHD model by the following two methods: Surface flux transport & Time-interpolation.

SFT Model

SIGMA Weather Group
太阳-行星际-地磁链
天气团队

- Applied to long-interval synoptic data products
  WSO, MDI(1 Carrington rotation cycle, 27 days)
- Differential rotation $\Omega(\theta)$& meridian flow $v(\theta)$

(1) Differential rotation

$$\Omega(\theta) = 0.18 - 2.3\cos^2\theta - 1.62\cos^4\theta \text{ deg day}^{-1}$$

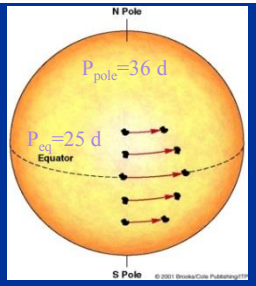

(2) Meridional flow

$$v_\theta(\theta) = C\cos\left[\frac{\pi(\theta_{\max} + \theta_{\min} - 2\theta)}{2(\theta_{\max} - \theta_{\min})}\right]\cos\theta$$

(3) Supergranular diffusion

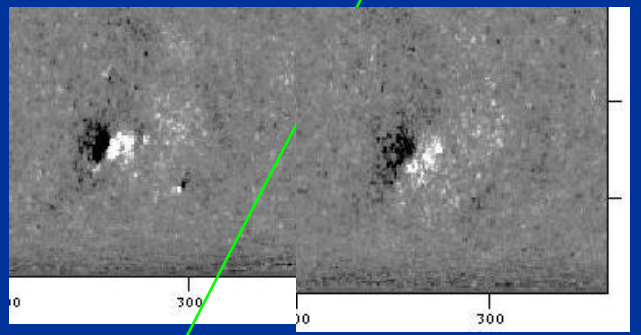

$$\frac{\partial B_r}{\partial t} = -\Omega(\theta)\frac{\partial B_r}{\partial \phi} - \frac{1}{R_S \sin\theta}\frac{\partial}{\partial \theta}\left[v(\theta)B_r \sin\theta\right] + \frac{D}{R_S^2}\left[\frac{1}{\sin\theta}\frac{\partial}{\partial\theta}\left(\sin\theta\frac{\partial B_r}{\partial\theta}\right) + \frac{1}{\sin^2\theta}\frac{\partial^2 B_r}{\partial\phi^2}\right] + S(\theta,\phi,t)$$

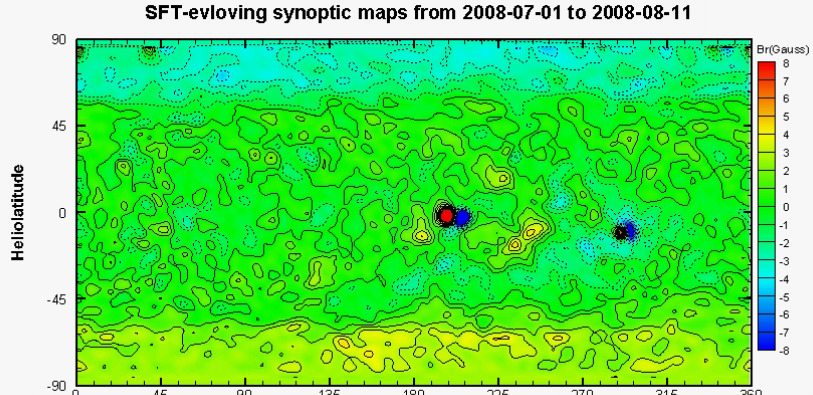

The surface flux transport (SFT) model describes the radial component evolution of large-scale photospheric magnetic field with time by using the magnetic induction equation in spherical coordinates. The flux transport model (Yeates, ApJ, 2010) accounts for known flows in the solar photosphere by including diff rotation & meridian flow.

Time Interpolation

- Applied to short-interval synoptic data products
  - GONG(6-hour), SDO-HMI(1-day)
- Using three synoptic maps to achieve third-order interpolation

$$B_r(t) = \frac{(t-t_2)(t-t_3)}{(t_1-t_2)(t_1-t_3)} B_{r,1} + \frac{(t-t_1)(t-t_3)}{(t_2-t_1)(t_2-t_3)} B_{r,2} + \frac{(t-t_1)(t-t_2)}{(t_3-t_1)(t_3-t_2)} B_{r,3}$$

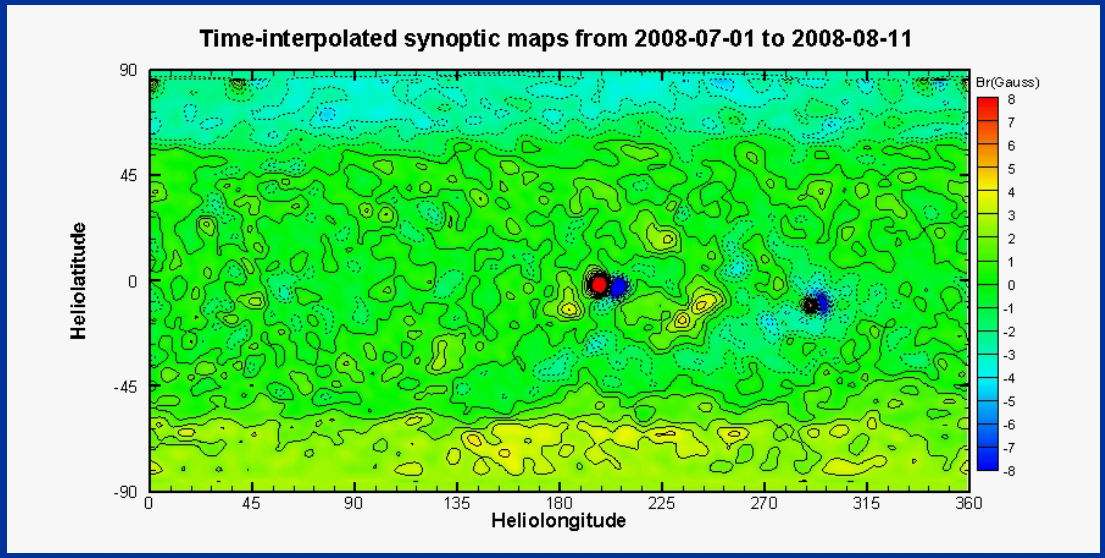

This data processing method is aimed to provide snapshot of magnetic maps

Roadmap

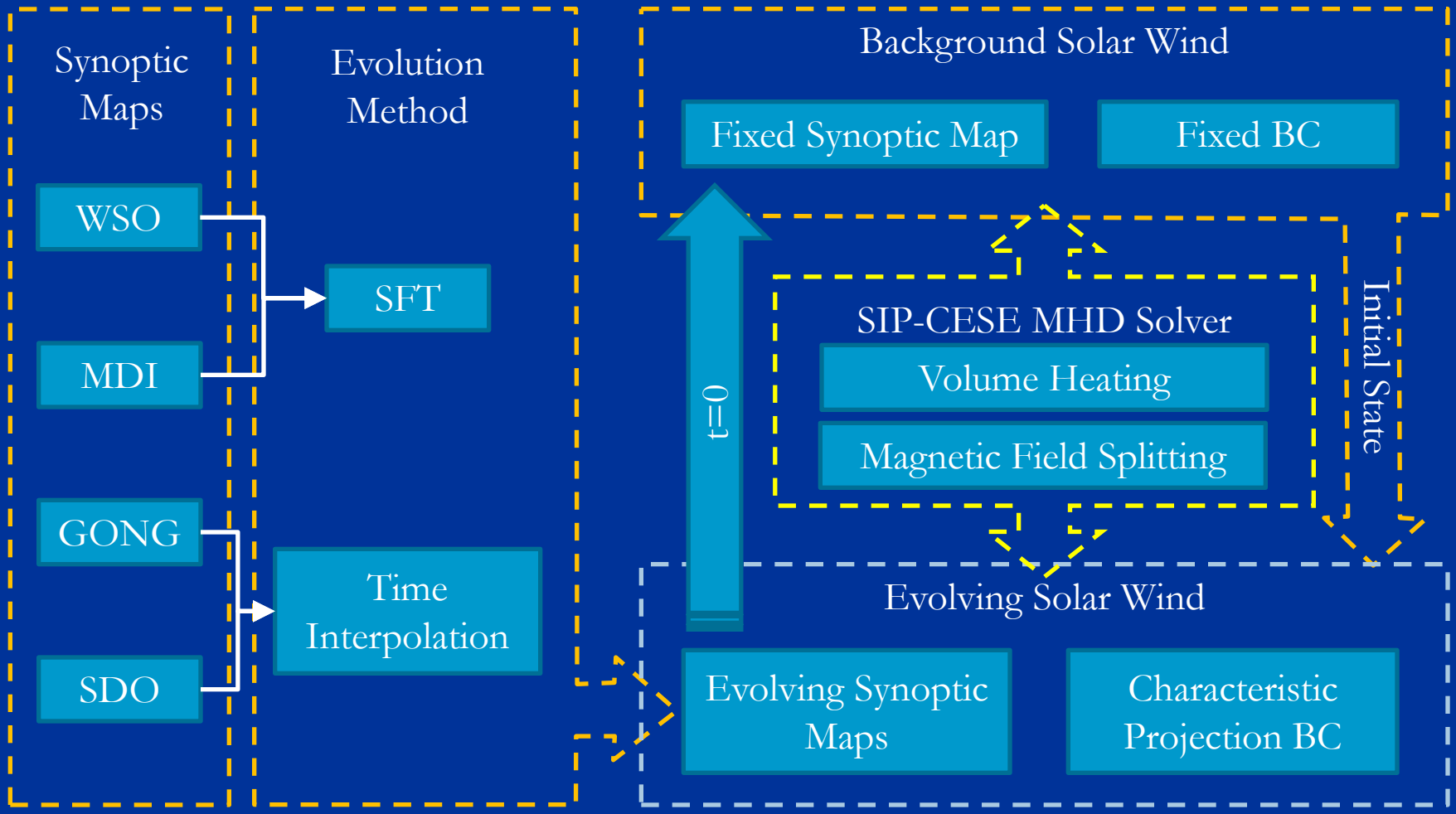
Synoptic Maps
Evolution Method
WSO
MDI
GONG
SDO
SFT
Time Interpolation
Background Solar Wind
Fixed Synoptic Map
Fixed BC
t=0
SIP-CESE MHD Solver
Volume Heating
Magnetic Field Splitting
Initial State
Evolving Solar Wind
Evolving Synoptic Maps
Characteristic Projection BC

Data-driven Method

- Obtain background solar wind
  - Fixed synoptic map(t=0)
  - Fixed boundary condition
  - Evolves(relaxes) until it reaches a steady state

  Based this steady-state, our data-driven procedure starts!
- Data-driven Solar Wind
  - Initialized with background solar wind obtained above
  - Evolving synoptic maps (SFT or time interpolation) for specific period (such as 2008-07-01 to 2008-08-11 below)
  - Projected characteristic boundary conditions at 1Rs

(Feng et al, ASTRONUM 2011; Feng et al, APJ, 2012; Yang et al., JGR, 2012)

Simulation Results From 2008-07-01 to 2008-08-11

SIGMA Weather Team
空间天气学国家重点实验室

- GONG 6-hour synoptic maps
- Third-order time interpolation
- From 2008-07-01 to 2008-08-11
- Can be continued with more synoptic map input

Iso-surface of Br=0

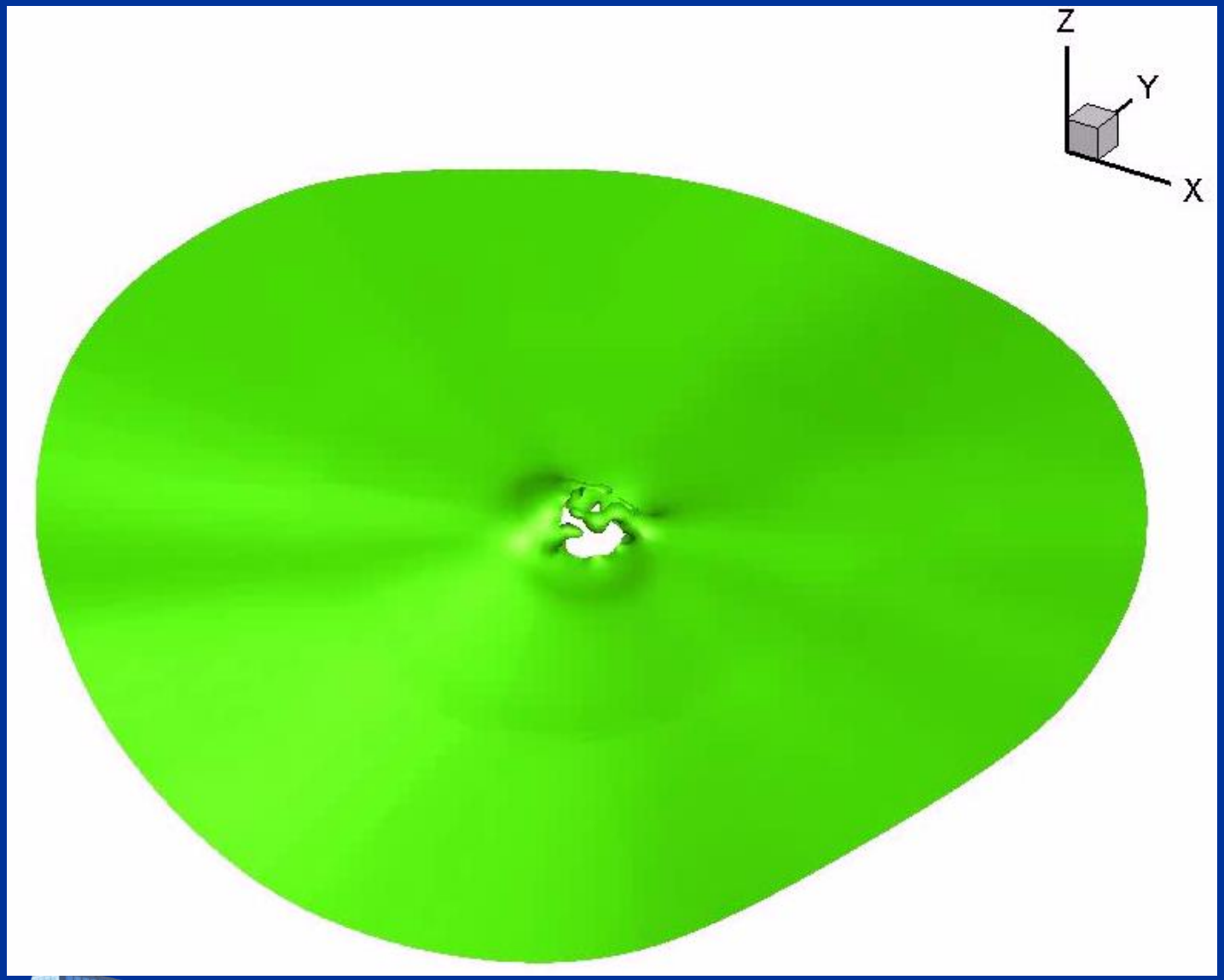

Corona Magnetic Field

SIGMA Weather Team
空间天气学国家重点实验室

3D Magnetic field on July 01, 08, 16, 23 and August 01, 08, 2008

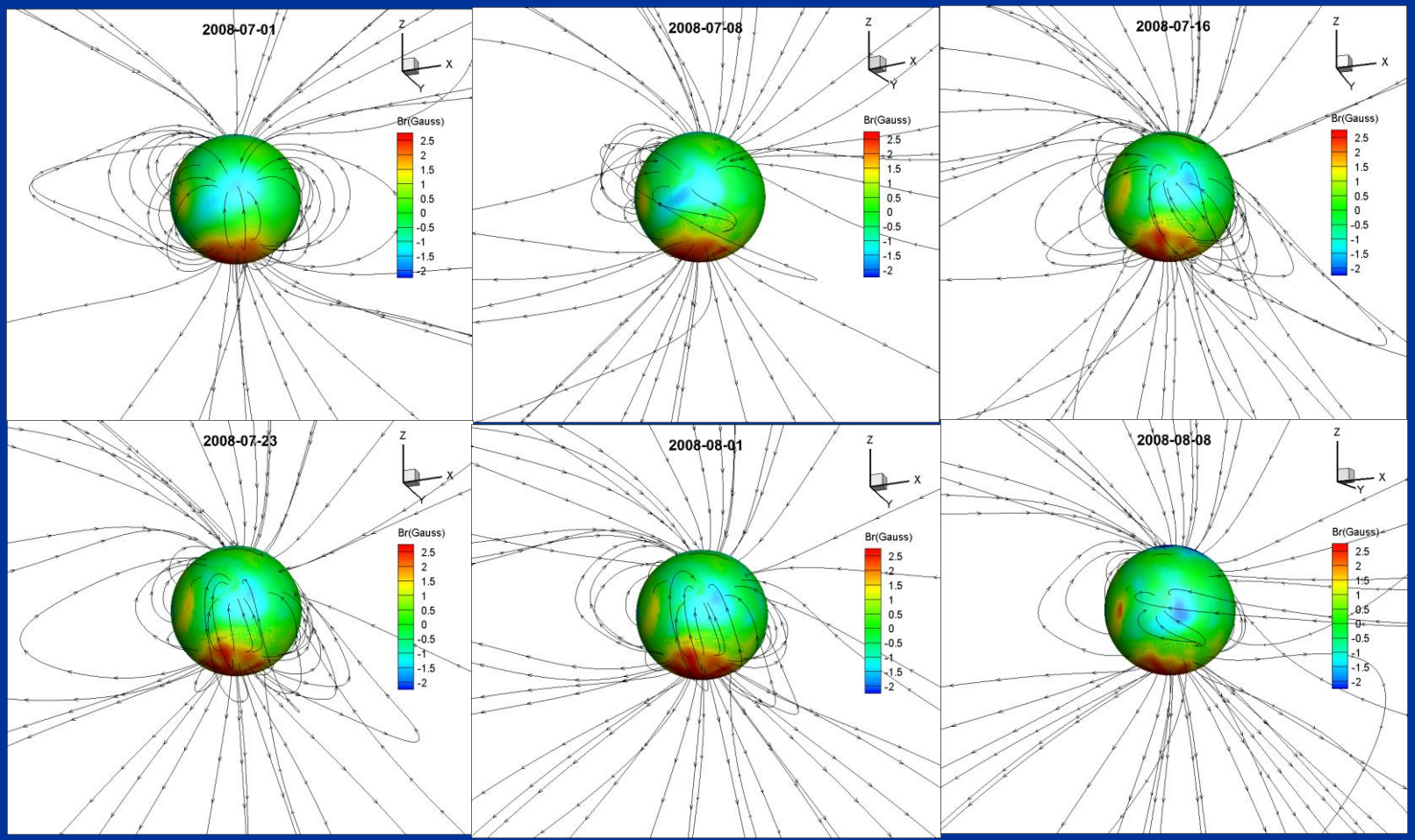

Contours at 2.5Rs

Number density

radial speed

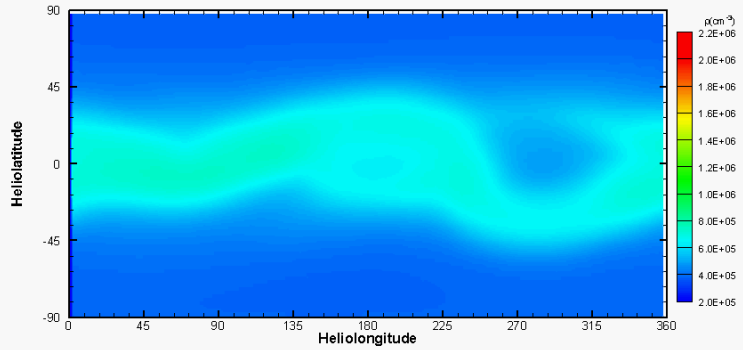

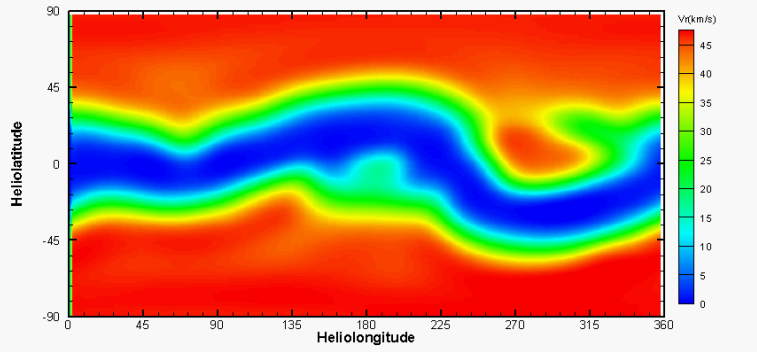

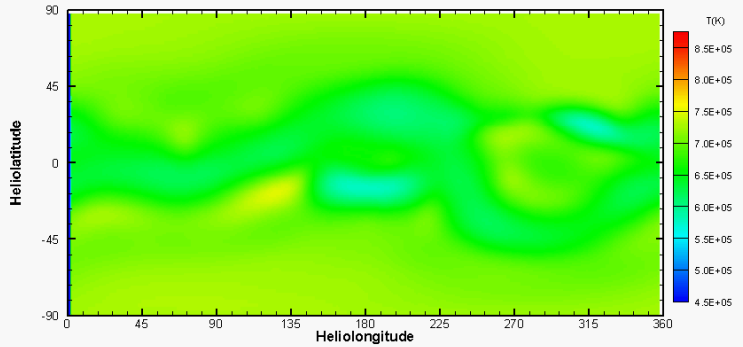

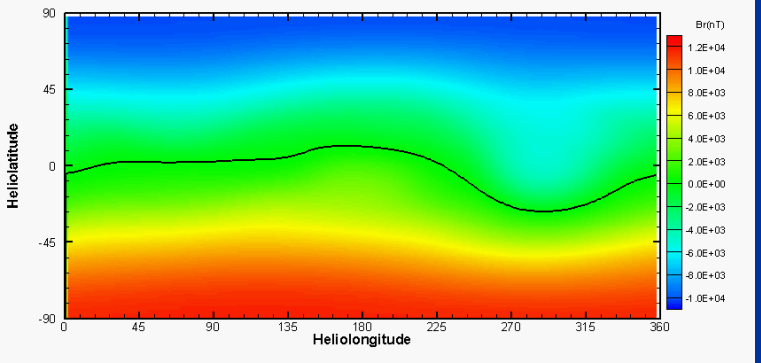

Temperature

Br

Contours at 0.1AU

Number density

radial speed

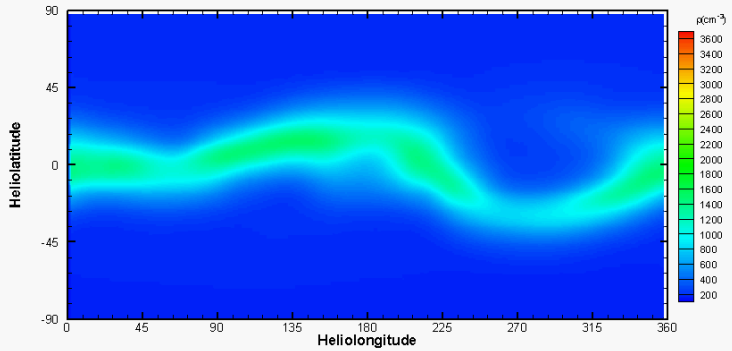

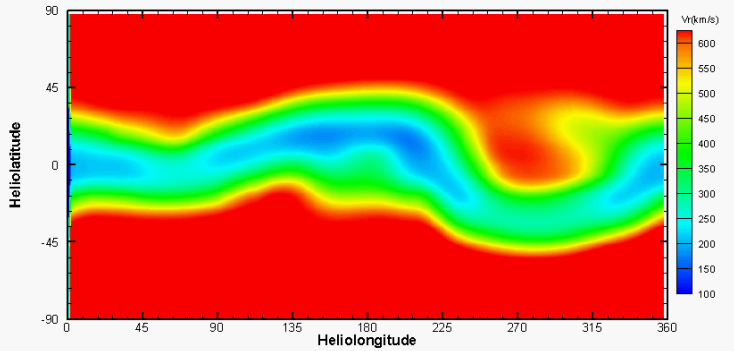

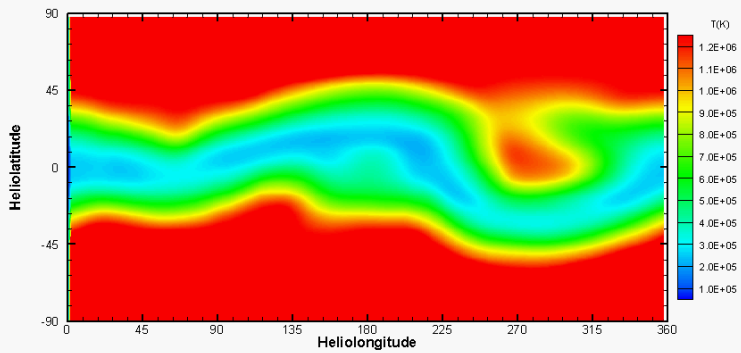

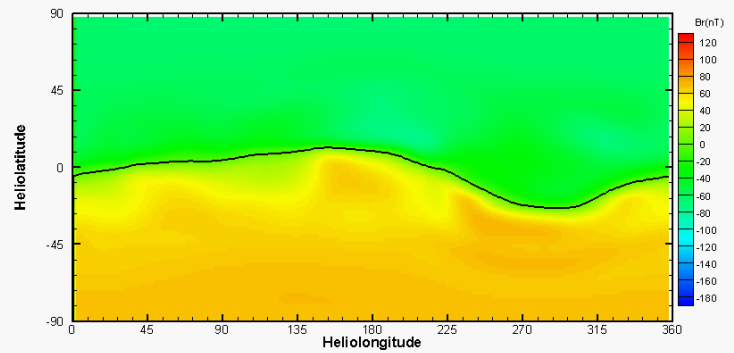

Temperature

Br

Contours at 1AU

Number density

radial speed

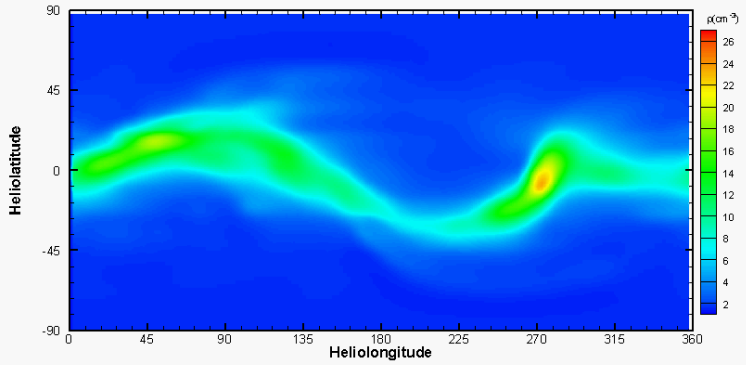

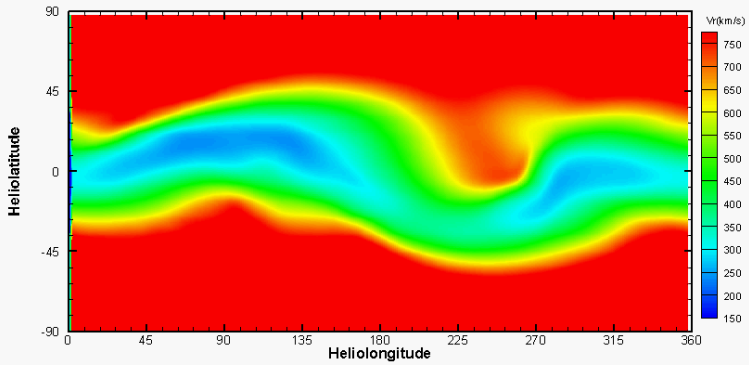

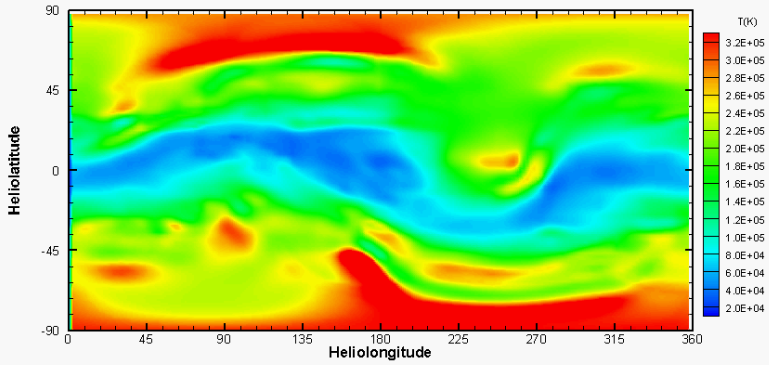

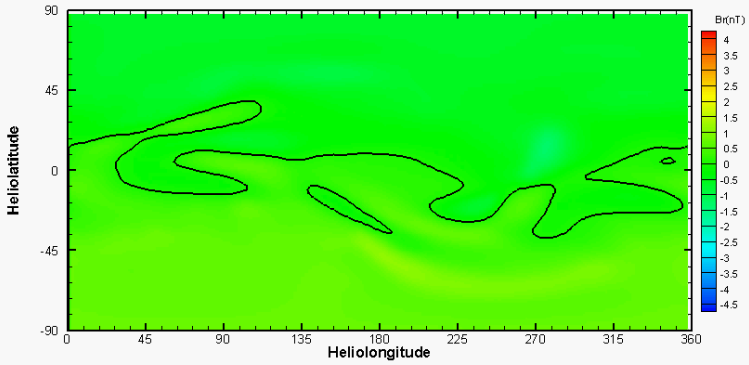

Temperature

Br

Compared with OMNI Data at 1AU

Radial speed

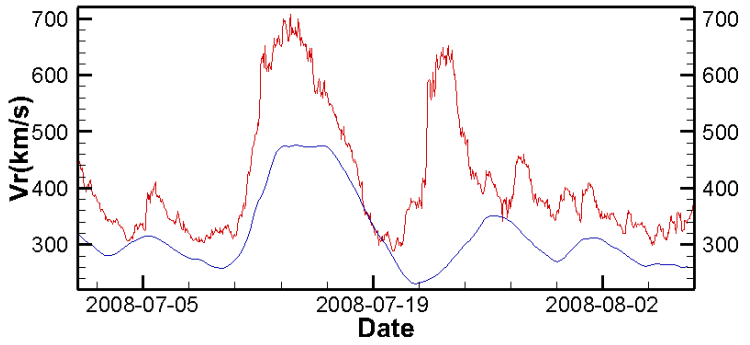

Number density

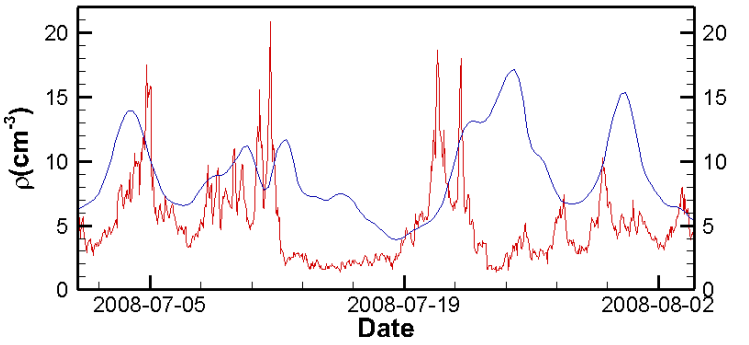

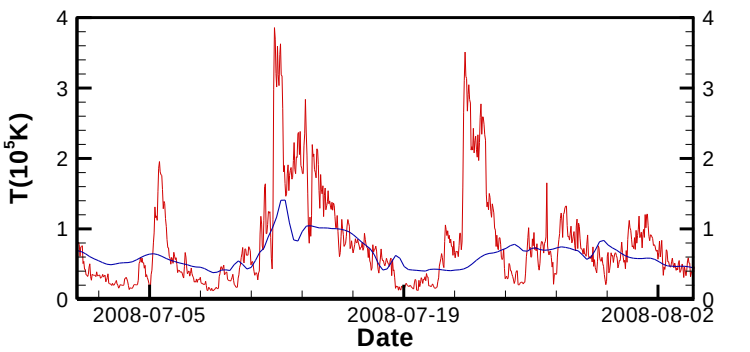

Temperature

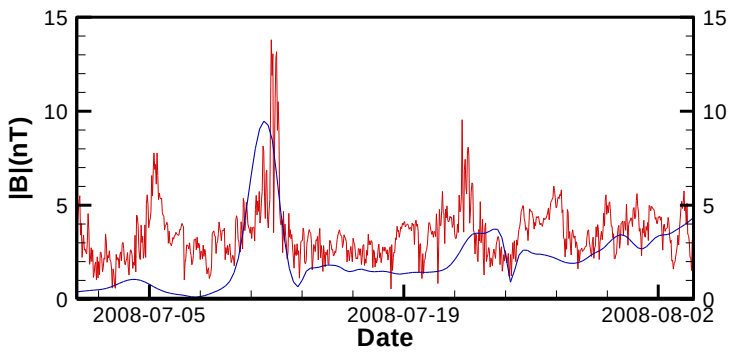

B

Equatorial plane

Radial speed

Mass flux $\rho V_r r^2$

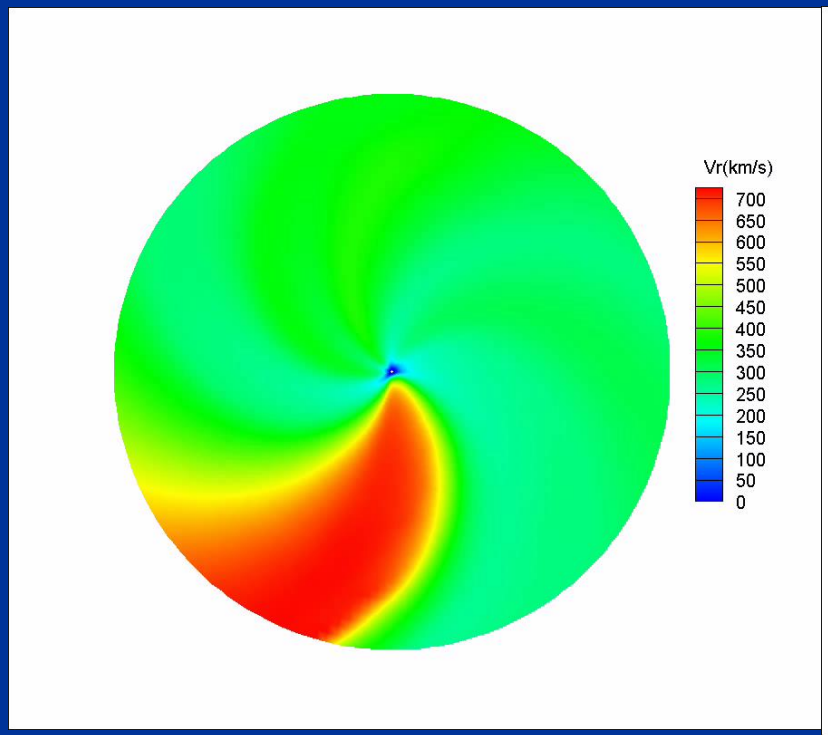

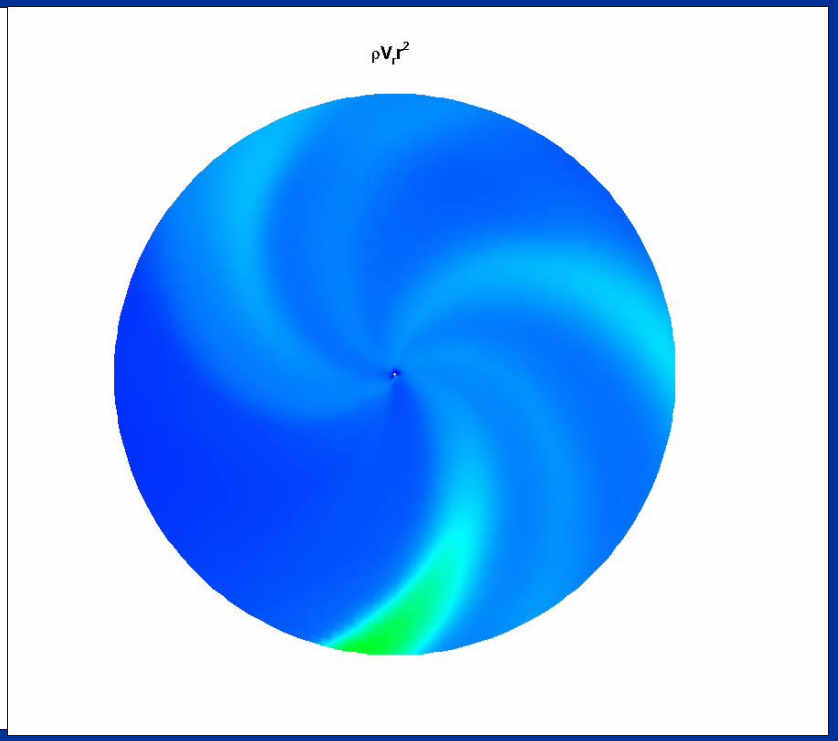

Meridian plane(YZ plane)

Radial speed

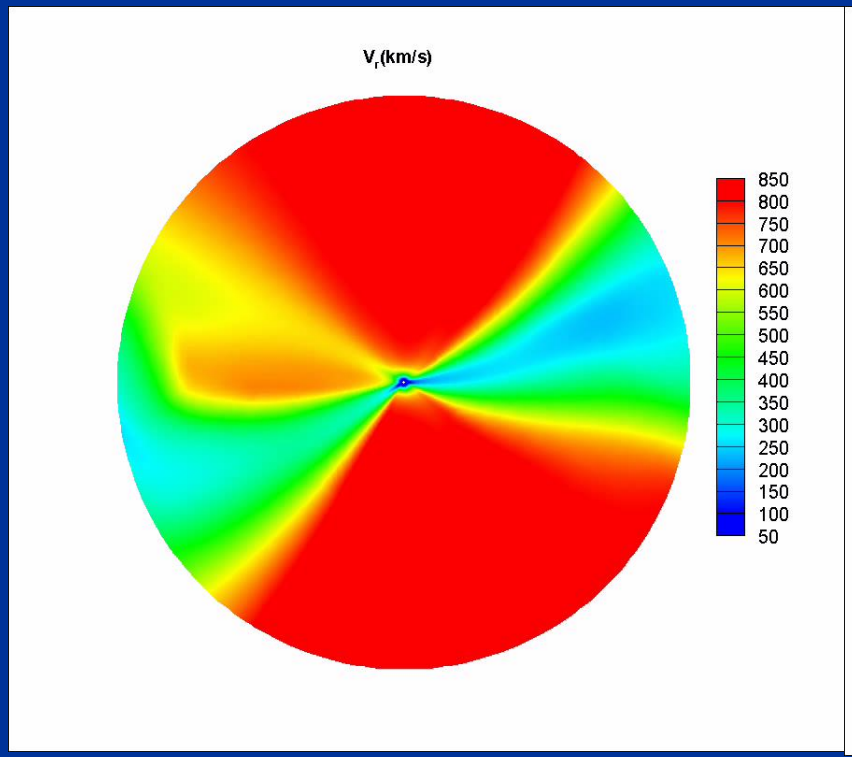

Mass flux $\rho V_r r^2$

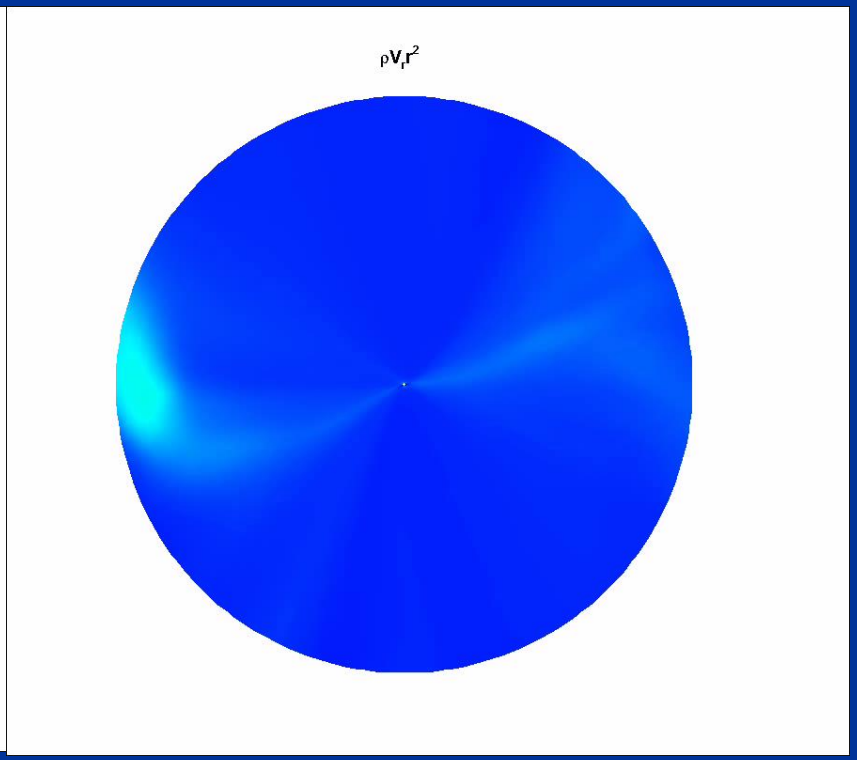

Meridian Plane (XZ plane)

SIGMA Weather Team
空间天气学国家重点实验室

Radial speed

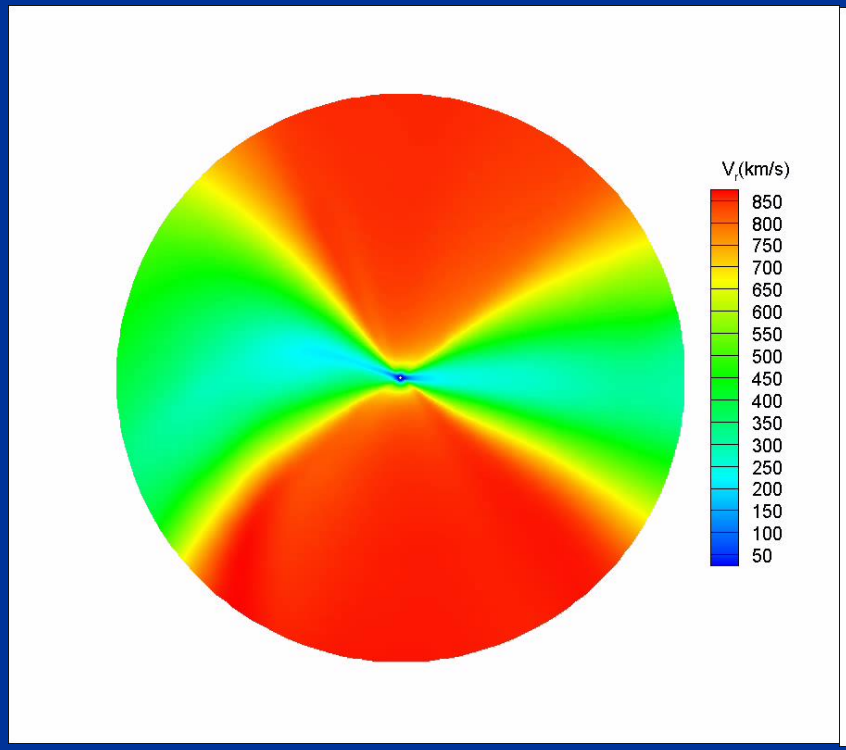

Mass flux $\rho V_r r^2$

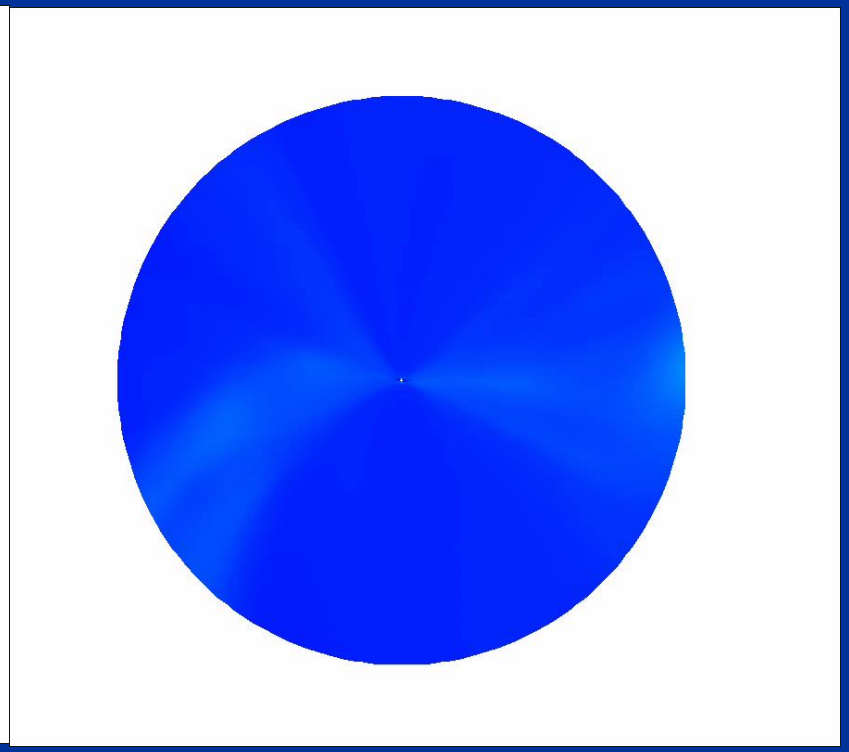

Corona Brightness

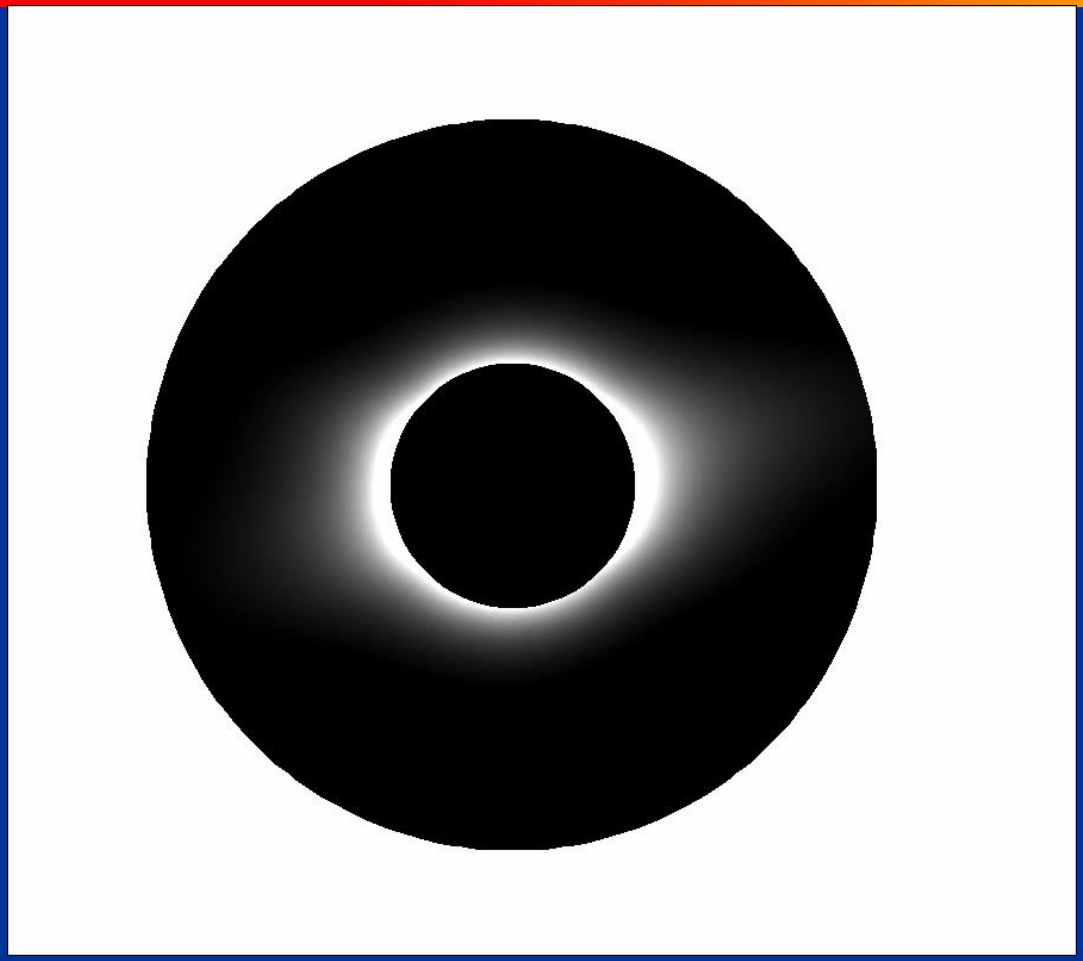

Summary

- With observed magnetic field data as input, this model can be able to simulate long-term evolution of solar wind (several Carrington rotations or even longer).
- This model is able to give solar wind parameters from corona to 1AU, which shows obvious time-dependent structures of the solar wind.
- Higher resolution magnetic data will achieve more agreement with observation

III. Data-Driven Numerical Modeling for Active Region Evolutions and Eruptions

SIGMA Weather Group
太阳-行星际-地磁链
天气团队

- Understanding how the solar coronal magnetic fields evolve and why the coronal fields erupt to produce flares and coronal mass ejections (CMEs), is a fundamental question of solar physics and it is crucial in forecasting space weather.
- We have developed a suite of numerical models for the magnetic evolution of the corona, including a unified and extremely fast code GLFFF for computing the global potential and linear force-free fields, a general nonlinear force-free extrapolation code CESE–MHD–NLFFF for both the local active regions and global corona, and a data-driven CESE–MHD model for simulating the magnetic evolution prior to and during eruptions.
- Based on these models & the booming data provided by SDO, a realistic 3D magnetic evolution for an eruption event from all over its formation to disruption can be achieved.

These lead to understanding how the eruptive core field is built up, the favorable magnetic topology is formed, and how the eruptions are triggered and driven.

Roadmap

SIGMA Weather Group
太阳-行星际-地磁链
天气团队

Data-Driven Numerical Models for the Evolution and Eruption of Solar Coronal Magnetic Field

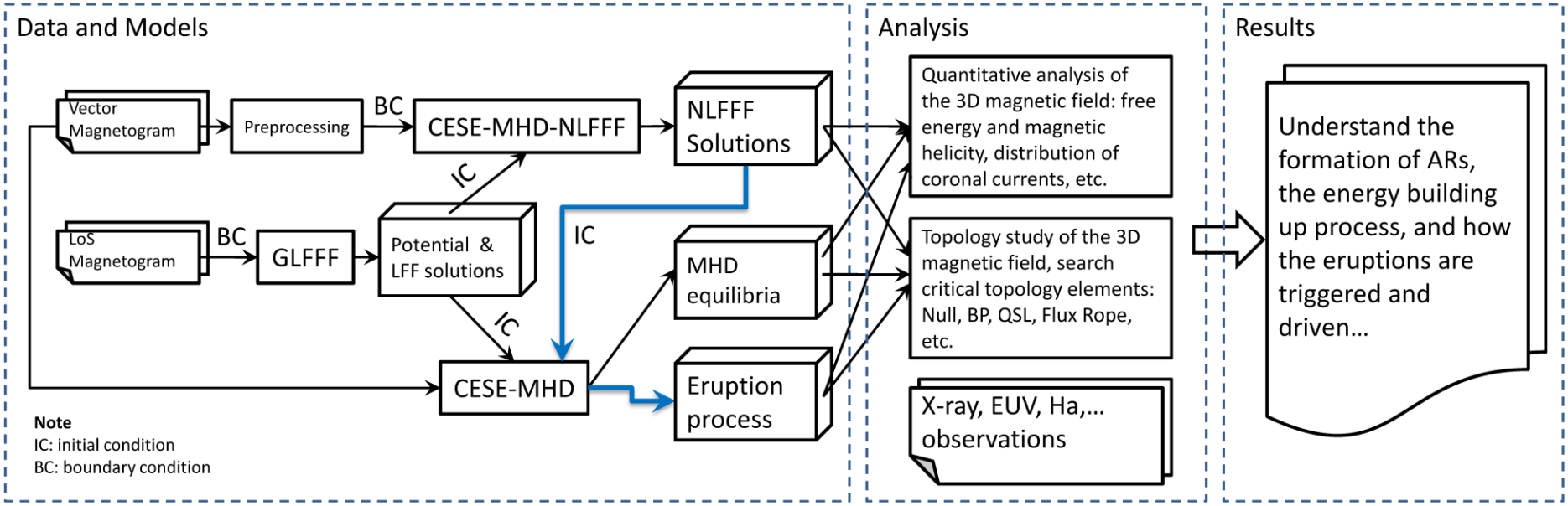

Note:

- **GLFFF: A very fast way for computing the global potential and linear force-free (LFFF) fields. Jiang & Feng (2012), Solar Physics**
- **CESE-MHD-NLFFF: A new implementation of the MHD-relaxation method for nonlinear force-free field (NLFFF) extrapolation Jiang & Feng, ApJ, 2012a, 2012b, 2013; Solar physics, 2013**
- **CESE-MHD: A data-driven MHD model for AR's magnetic evolution Jiang & Feng et al 2012, ApJ; 2013, ApJL.**

As an example, using a nonlinear force-free field extrapolation prior to a sigmoid eruption in AR 11283 as the initial condition in a MHD model, we successfully simulate the realistic initiation process of the eruption event, as is confirmed by a remarkable resemblance to the SDO/AIA observations.

Analysis of the pre-eruption field reveals that the envelope flux of the sigmoidal core contains a coronal null and furthermore the flux rope is prone to a torus instability, as suggested by observations. This kind of simulation demonstrates the capability of modeling the realistic solar eruptions to provide the initiation process.

CESE-MHD-NLFFF extrapolation (Jiang & Feng, ApJ, 2013, 769, 144)

SIGMA Weather Group
太阳-行星际-地磁链
天气团队

Main Equation (modified magneto-frictional model in the magnetic splitting form)

$$\frac{\partial \rho \mathbf{v}}{\partial t} = (\nabla \times \mathbf{B}_1) \times \mathbf{B} - (\nabla \cdot \mathbf{B}_1)\mathbf{B} - \nu \rho \mathbf{v},$$

$$\frac{\partial \mathbf{B}_1}{\partial t} = \nabla \times (\mathbf{v} \times \mathbf{B}) + \nabla(\mu \nabla \cdot \mathbf{B}_1) - \mathbf{v} \nabla \cdot \mathbf{B}_1,$$

$$\rho = |\mathbf{B}|^2 + \rho_0, \quad \mathbf{B} = \mathbf{B}_0 + \mathbf{B}_1.$$

Extrapolation test of the van Ballegooijen (2004) flux rope model (Jiang & Feng, ApJ 2012a)

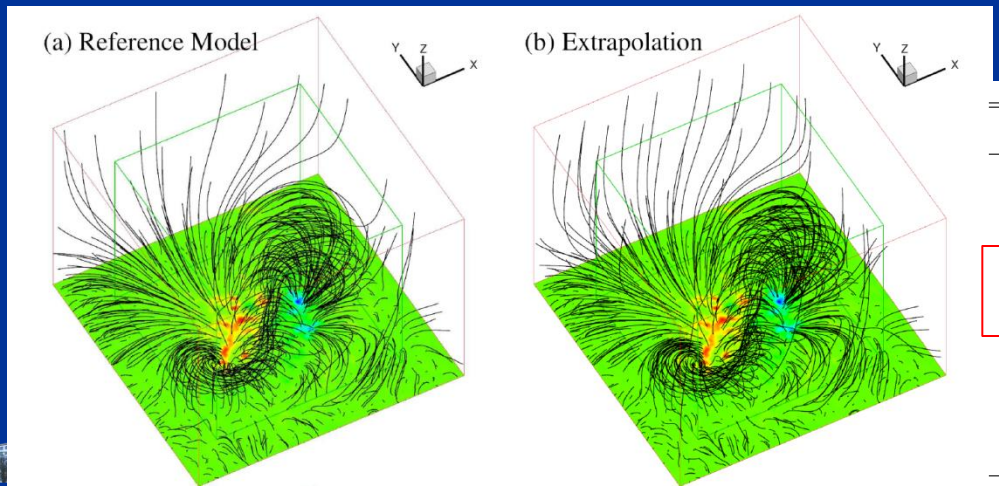

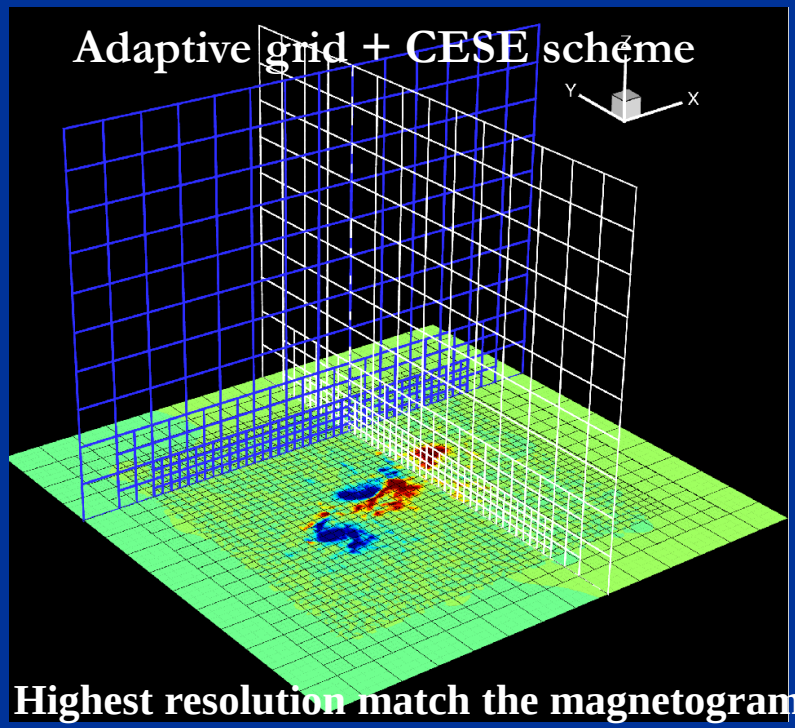

Highest resolution match the magnetogram (e.g., 0.5 arcsec for HMI data); coarsest resolution ~4 arcsec

Model	C_{vec}	C_{CS}	E'_{n}	E'_{m}	E/E_{pot}	CWsin	$\langle \lvert f_i \rvert \rangle$
For $z \in [2, 225]$							
Reference	1.000	1.000	1.000	1.000	1.343	0.107	1.02×10^{-4}
Our result	0.995	0.978	0.885	0.734	1.337	0.133	1.11×10^{-4}
Wiegelmann*	1.00	0.99	0.89	0.73	1.34	0.11	
Wheatland*	0.95	0.98	0.79	0.70	1.21	0.15	
Valori*	0.98	0.98	0.84	0.71	1.25	0.15	
Potential	0.852	0.952	0.687	0.665	1.000		

Formation and Eruption of a Sigmoid in AR 11283

SIGMA Weather Group
太阳-行星际-地磁链
天气团队

- AIA observation of the emergence and eruption

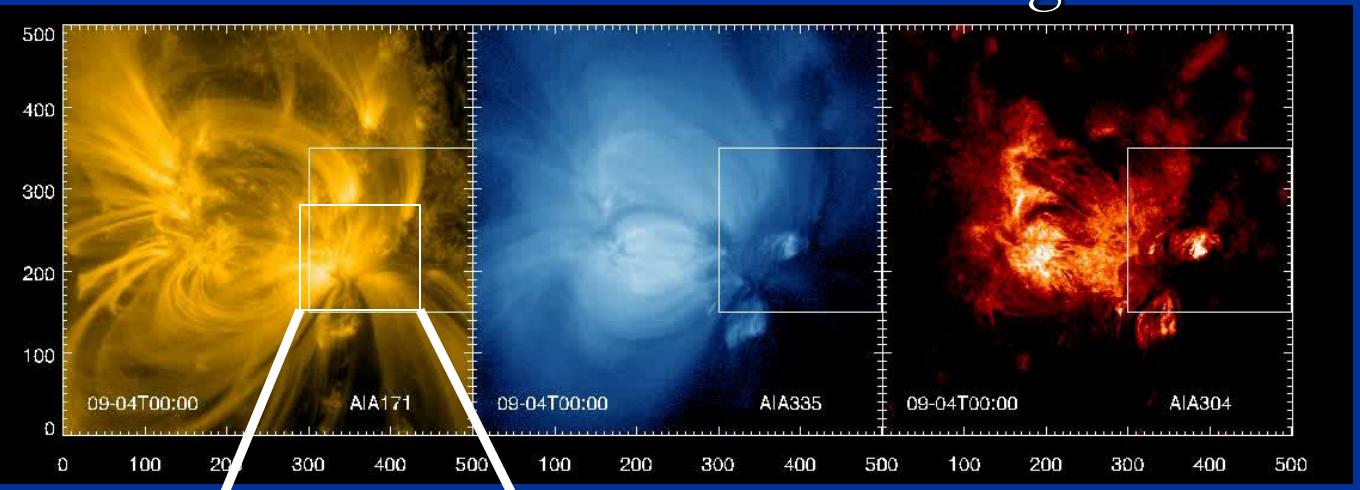

AR 11283 (2011/09/04-06)

➢ From 2011/09/04: New flux emergence into a bipolar active region

AIA 171, 335, 304

AIA 094

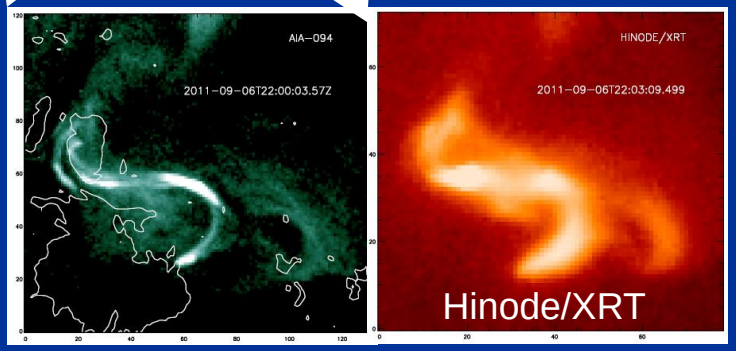

➢ 2011/09/06: A sigmoid formed around 22:00UT.

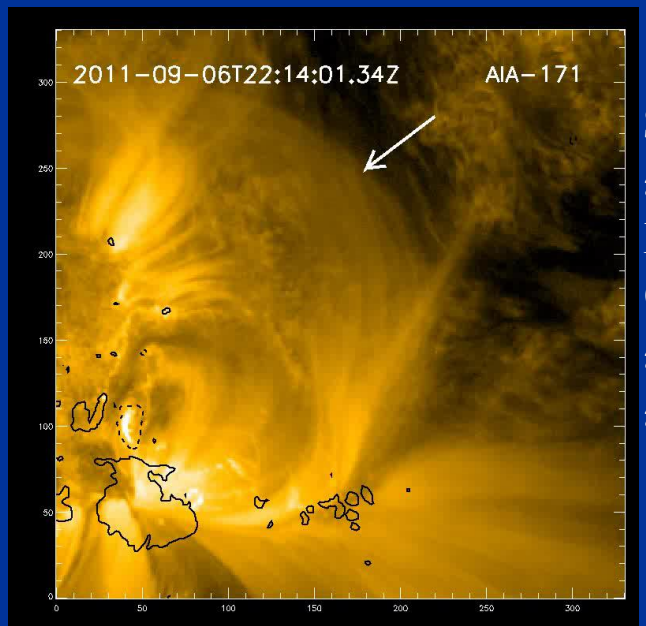

➢ 2011/09/06: Sigmoid eruption at 22:17UT, Developed to a CME, associated with a X2.1 flare

Formation and Eruption of a Sigmoid in AR 11283

SIGMA Weather Group
太阳-行星际-地磁链
天气团队

- Photospheric flux emergence
  - Before 2011-09-04: Simple mature, bipolar (P0/N0) AR.
  - After 2011-09-04: New bipolar (P1/N1) emergence

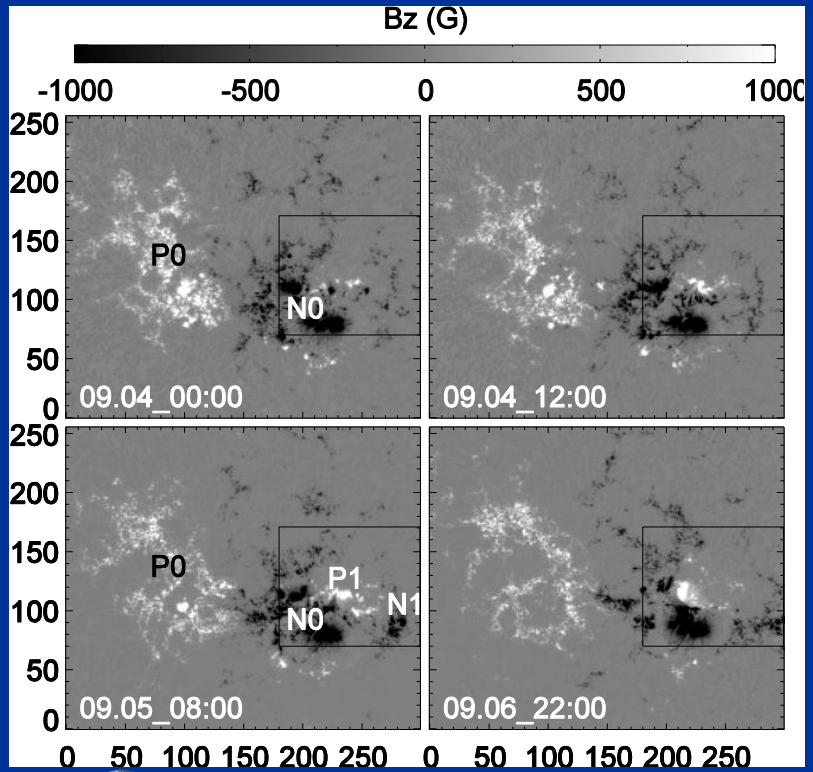

Evolution of the photoshperic field observed

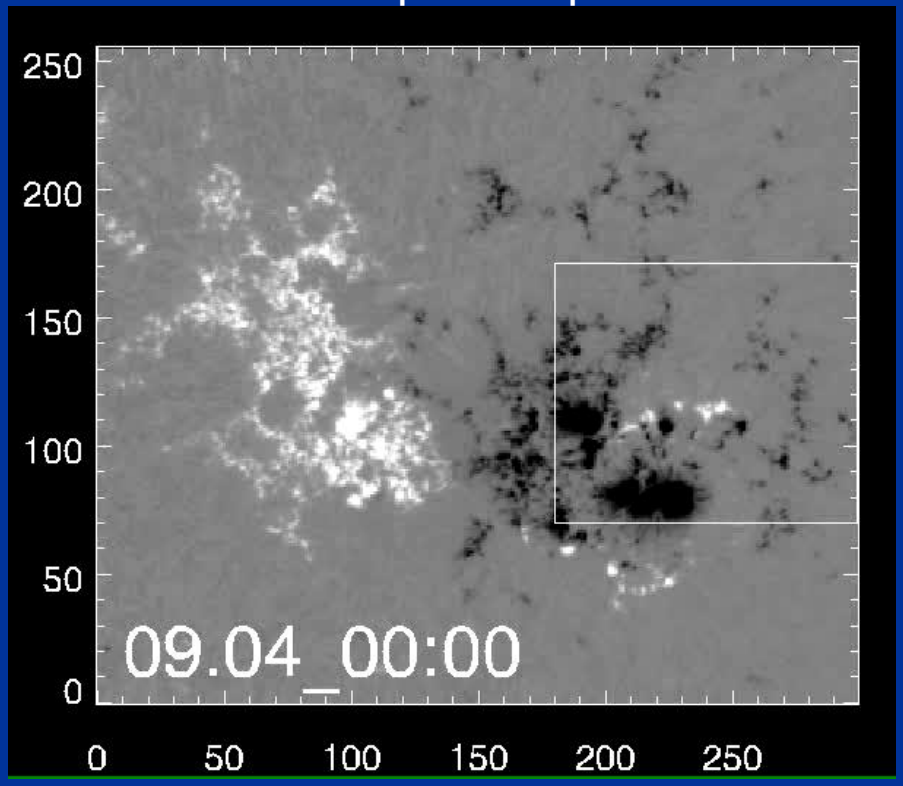

Field of view: 300*256 arcsec^2 (res=0.5arcsec)

Formation and Eruption of a Sigmoid in AR 11283

SIGMA Weather Group
太阳-行星际-地磁链
天气团队

- Photospheric signal of energy building up process
  - Apparent new flux injection occurred mostly on the first day (09/04).
  - Non-potentiality increased mostly on the second day (09/05), resulted by photospheric shear and rotation.

Total unsigned flux $\Phi = \int_S |Bz|ds$; Unsigned current $I = \int_S |Jz|ds$; (LSS=length of strong magnetic shear (>45 °) with strong transverse field (> 300 G)]

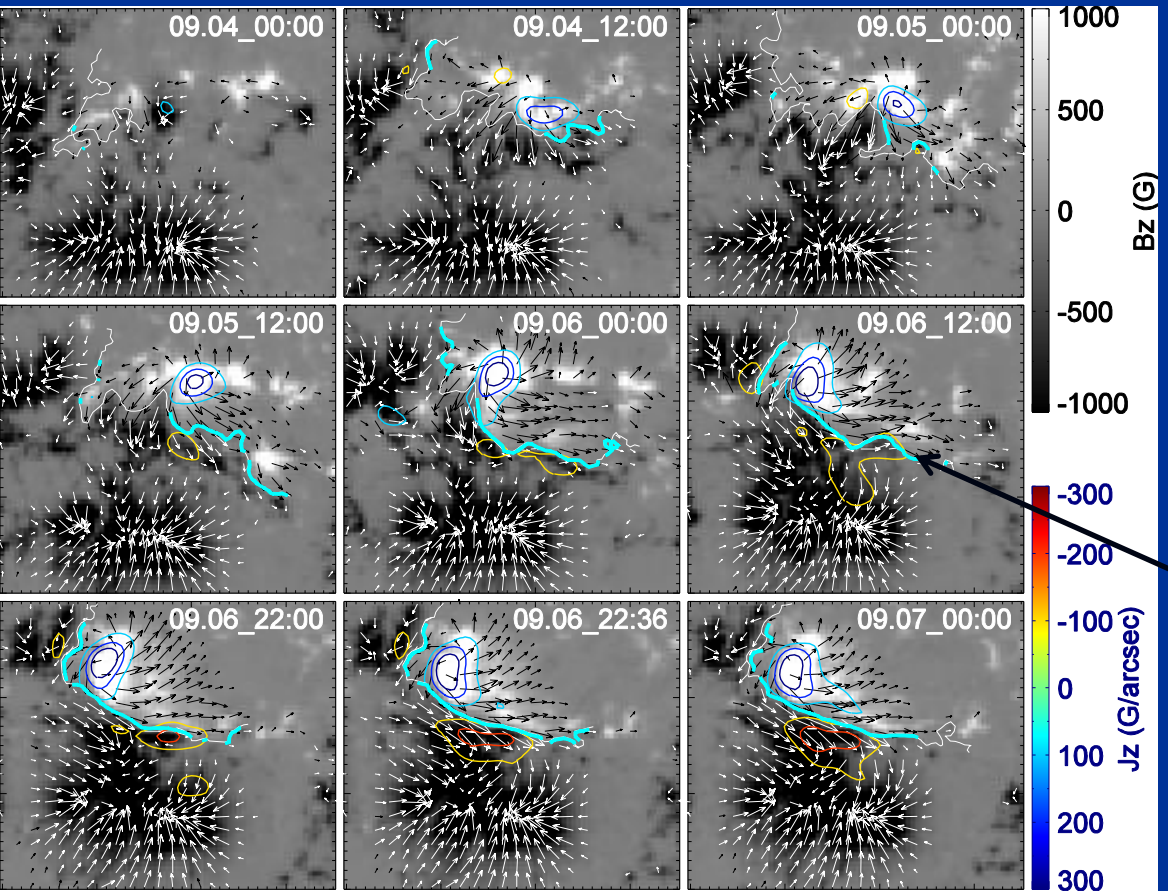

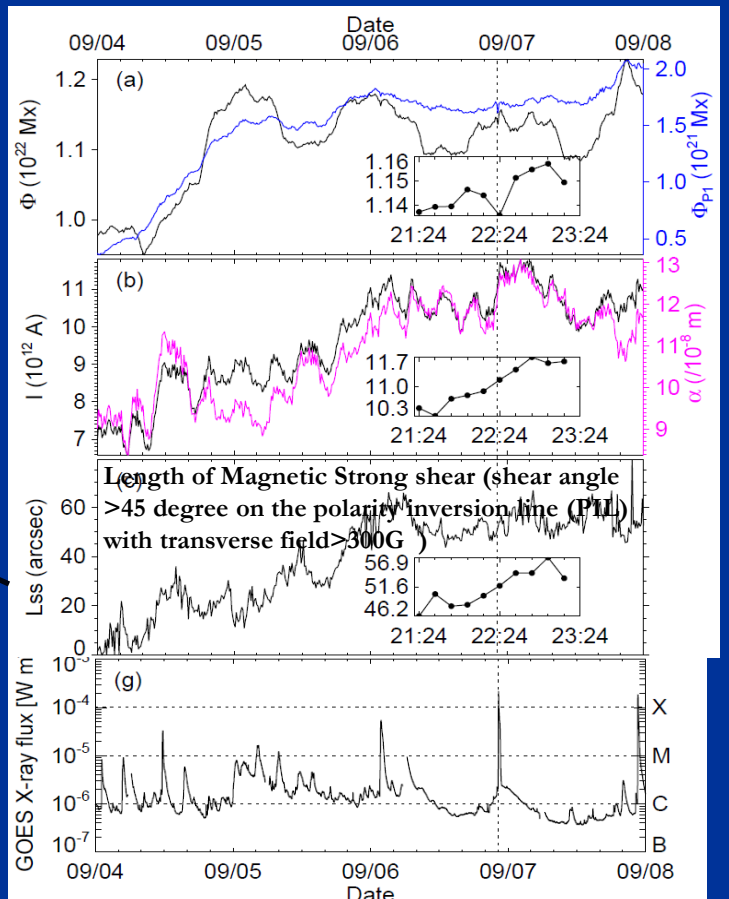

Formation and Eruption of a Sigmoid in AR 11283

SIGMA Weather Group
太阳-行星际-地磁链
天气团队

NLFFF modeling of the long-term quasi-static magnetic evolution

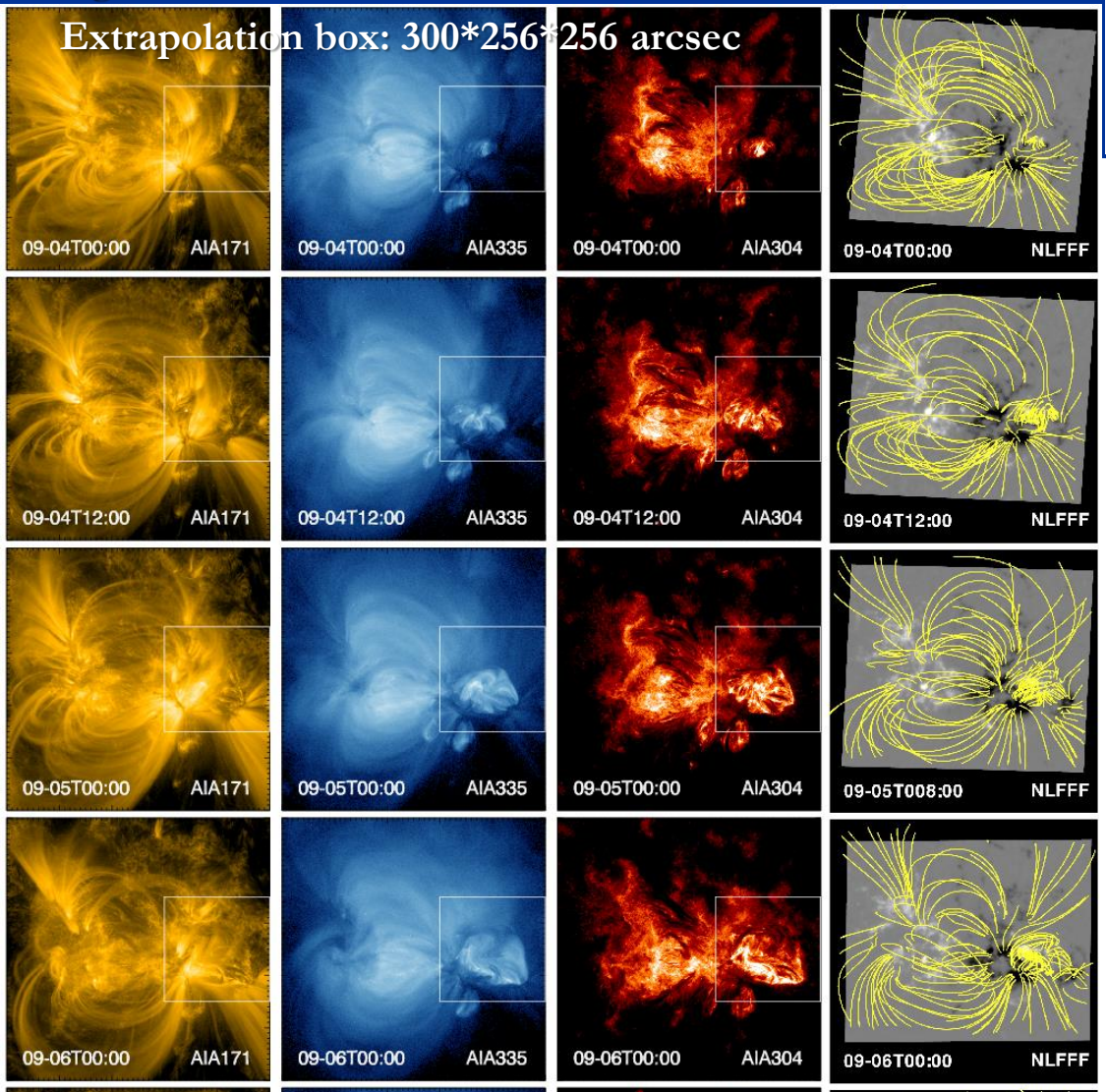

With the 3D coronal field, the volume energy can be computed. The energy that can be released by eruptions is the free energy $E_{\rm free}$, i.e., the total energy $E_{\rm tot}$ substracting the potential energy $E_{\rm pot}$

$$E_{\rm tot}=\int_V \frac{B^2}{8\pi}dV,\ E_{\rm pot}=\int_V \frac{B_{\rm pot}^2}{8\pi}dV,\ E_{\rm free}=E_{\rm tot}-E_{\rm pot} \quad (2)$$

where $B_{\rm pot}$ is the potential field strength. Different ener-

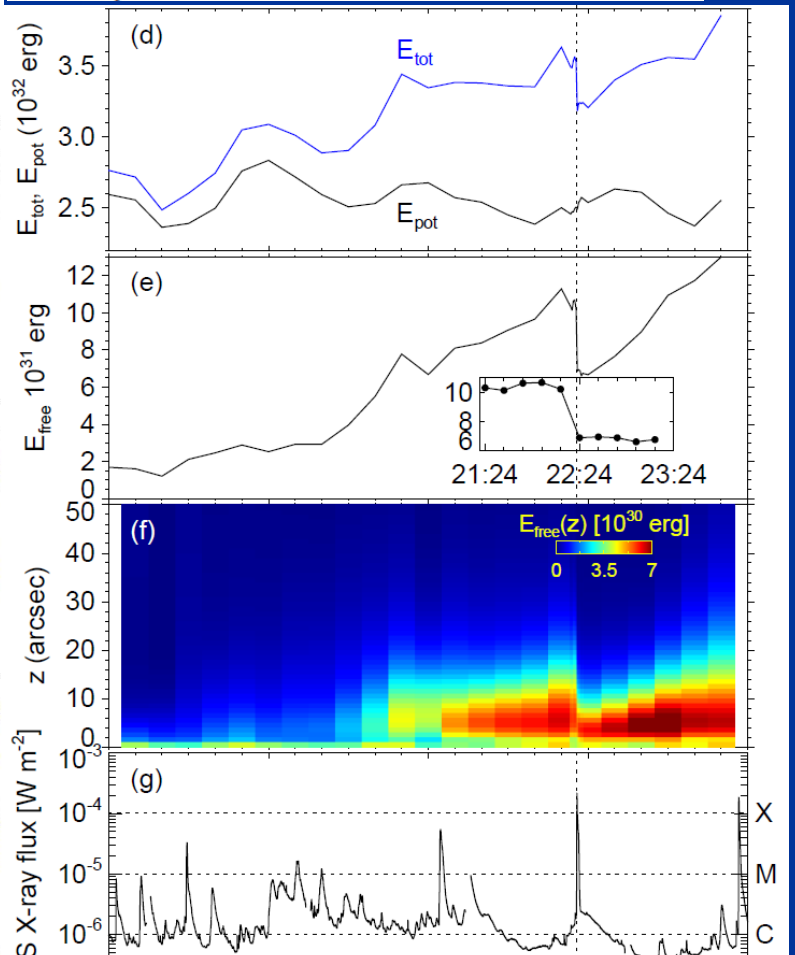

Formation and Eruption of a Sigmoid in AR 11283

SIGMA Weather Group
太阳-行星际-地磁链
天气团队

- Magnetic topology of the Sigmoid

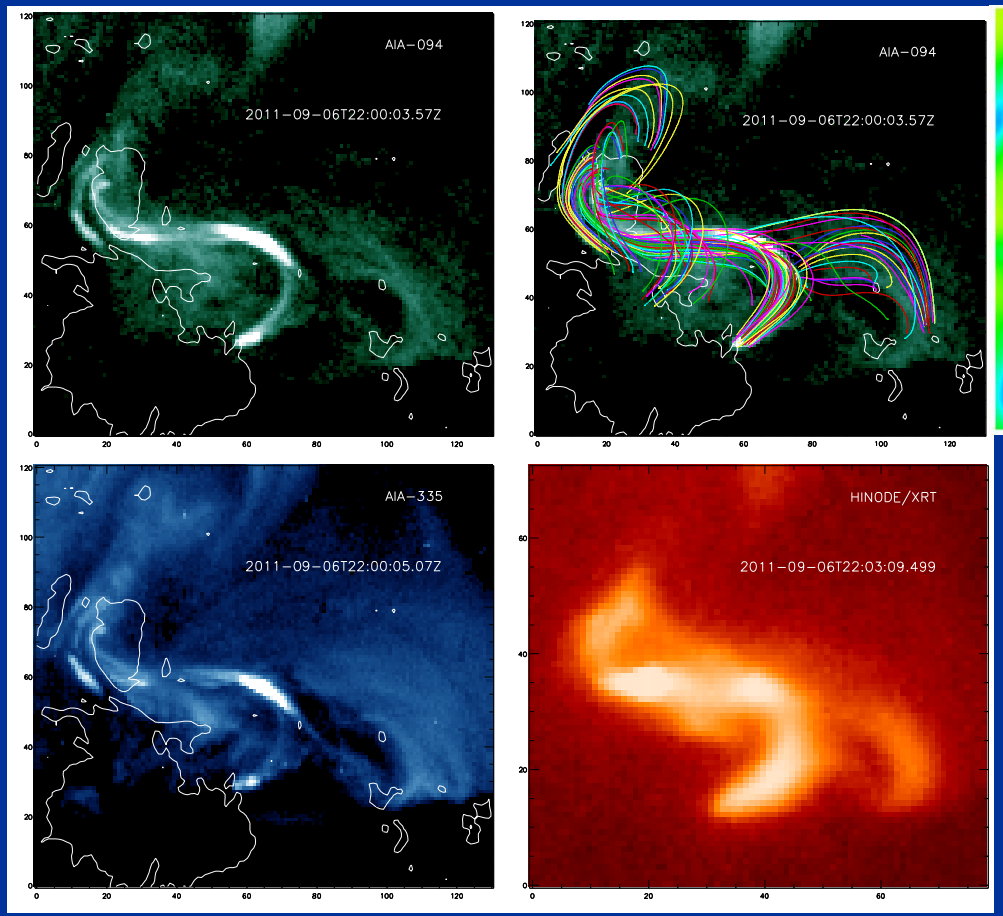

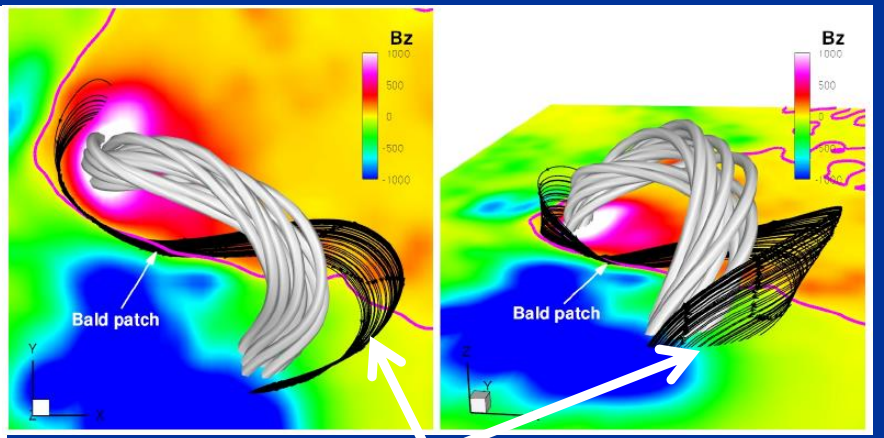

BPSS

➢ NLFFF reconstructs the sigmoid field very precisely!

➢ The closest resemblance to the observed sigmoid actually corresponds to the BPSS (Bald patch separatrix surface, i.e., field lines that graze the photosphere at BP, Titov & Démoulin 1999). Support the BPSS model of sigmoid (TD1999, Gibson2006).

Formation and Eruption of a Sigmoid in AR 11283

SIGMA Weather Group
太阳-行星际-地磁链
天气团队

- Formation of the basic topology and the sigmoidal flux rope

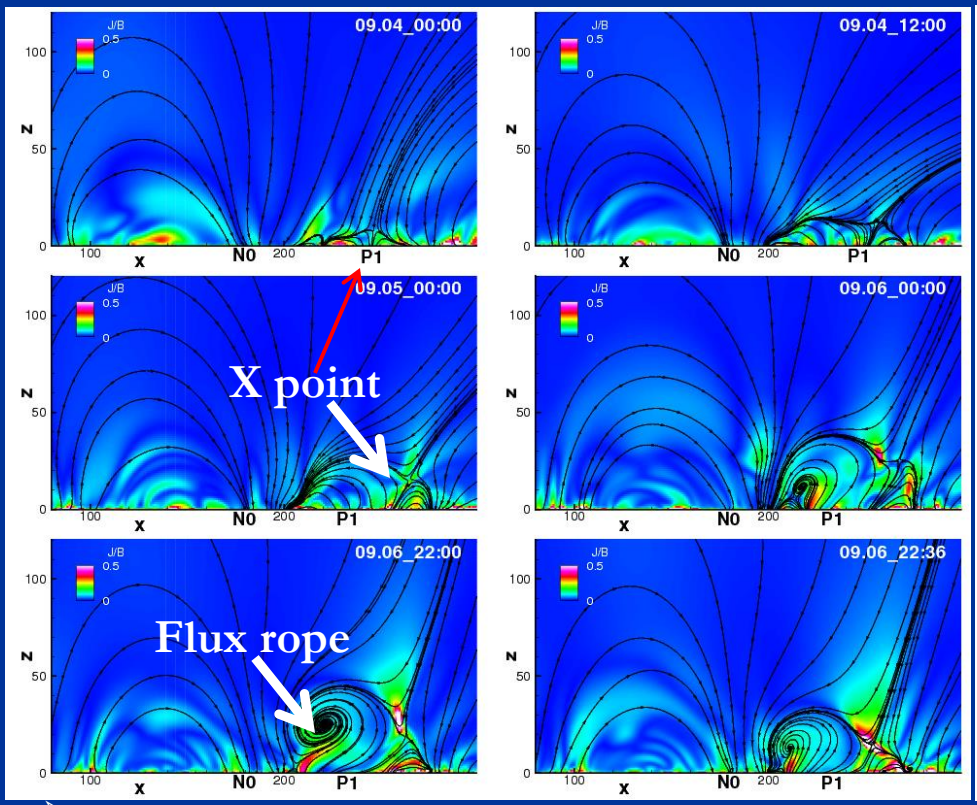

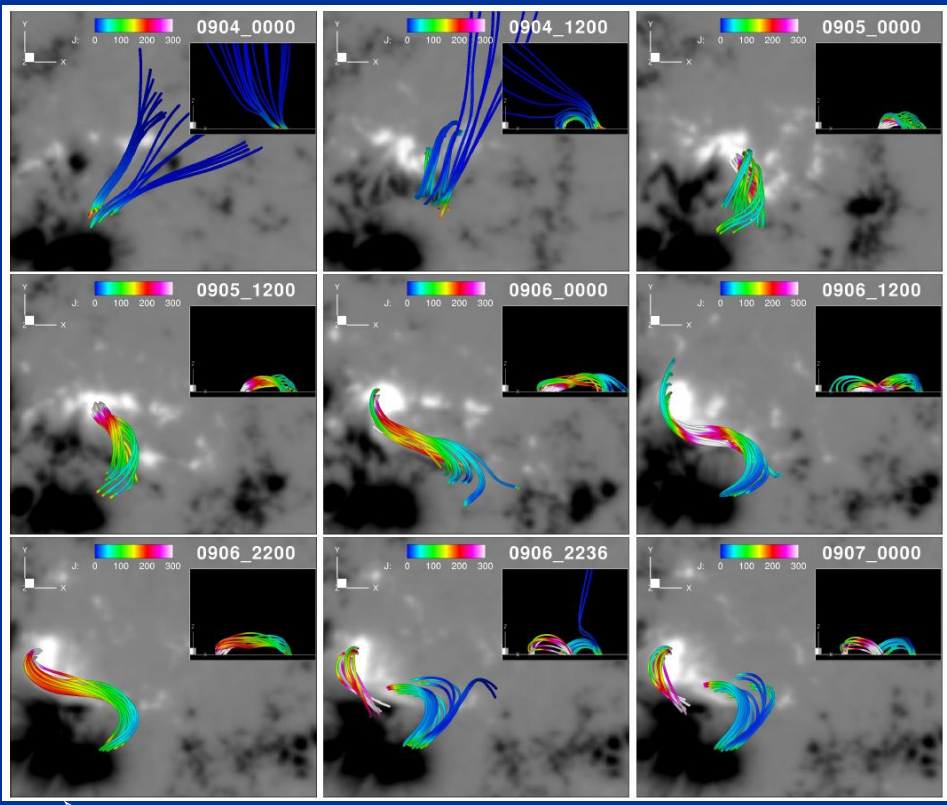

- Cross section of the 3D NLFFF data.
- An X point (coronal null in 3D) forms above the new polarity P1 and lift up
- A flux rope forms above the polarity inversion line (PIL)of P1/N0

- Photospheric shear change potential arcade to double-J shaped loop system;
- S-shaped flux rope formed from the double-J loops by tether-cutting reconnection (Moore et al. 2001).
- Flux rope disappeared after eruption

Eruption mechanism

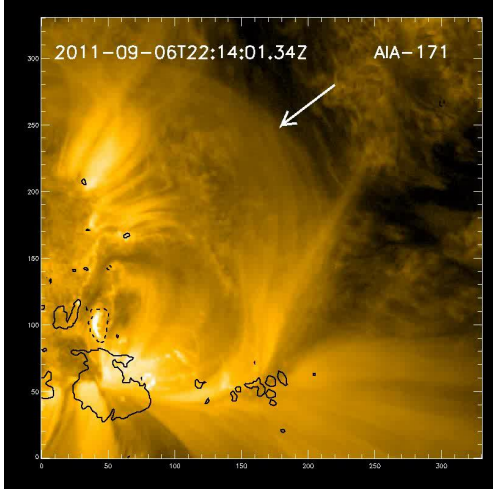

➢ Overlying flux of the sigmoid core contains a Coronal null

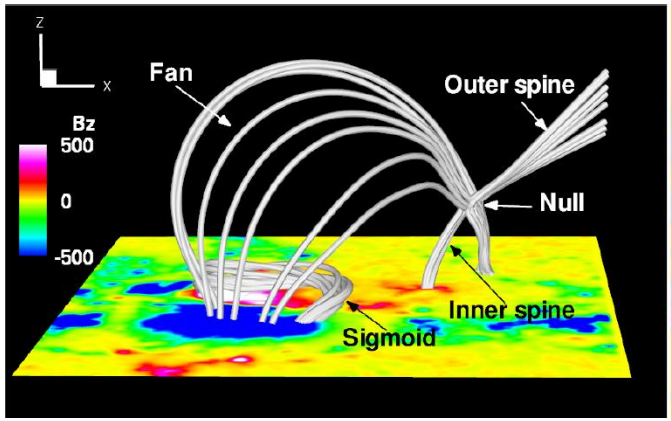

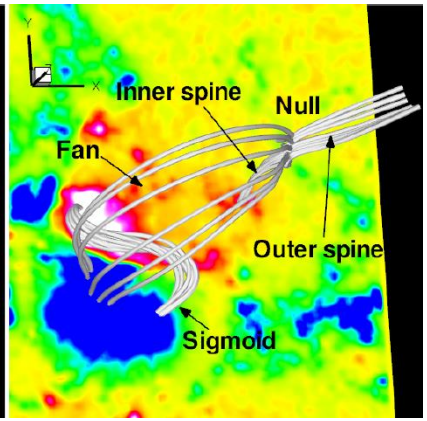

➢ Magnetic reconnection at the null cuts some overlying tethers (evidence: circular flare ribbon and overlying closed loops opened)→ Flux rope expand slightly→ TI is triggered →Fast eruption

➢ The flux rope—overlying flux system is prone to the Torus instability (TI, Kliem & Torok, 2006)

Streamlines: projection of 3D field lines
Color: field strength *B*

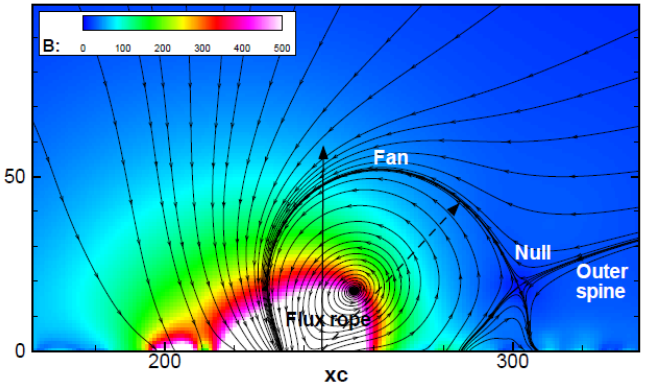

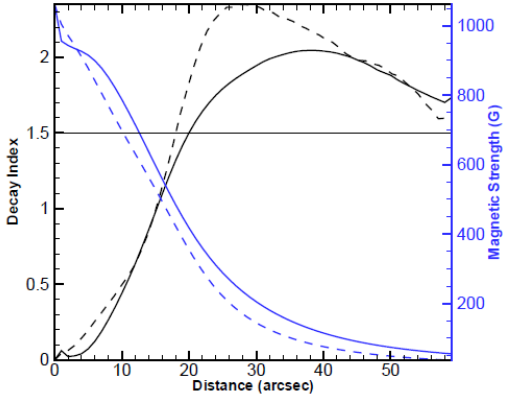

Decay speed of envelope flux defined decay index $decay\ index = -\frac{r}{B}\frac{\partial B}{\partial r}$

horizontal line at 1.5, a critical threshold for torus instability (Torok & Kliem 2007; Aulanier et al. 2009). Note that the flux rope reaches almost 20 arcsec (left Figure 11), a height with decay index > 1.5.

A vertical cross section cutting through the coronal null and the middle of the sigmoid, thus roughly parallel to the direction of eruption as observed. The thick solid and dashed lines with arrows denotes two directions (started from near the PIL on the bottom) in which the decay indexes of the field strength are plotted in right Figure. The solid one is radial and the dashed roughly the eruption direction modeled by the MHD simulation.

Data-Driven CESE-MHD Model

SIGMA Weather Group
太阳-行星际-地磁链
天气团队

MHD Equation

$$\frac{\partial \rho}{\partial t} + \nabla \cdot (\rho \mathbf{v}) = 0,$$

$$\rho \frac{D\mathbf{v}}{Dt} = -\nabla p + \mathbf{J} \times \mathbf{B} + \rho \mathbf{g} + \nabla \cdot (\nu \rho \nabla \mathbf{v}),$$

$$\frac{\partial \mathbf{B}}{\partial t} = \nabla \times (\mathbf{v} \times \mathbf{B}),$$

$$\frac{\partial T}{\partial t} + \nabla \cdot (T\mathbf{v}) = (2-\gamma) T \nabla \cdot \mathbf{v} + Q.$$

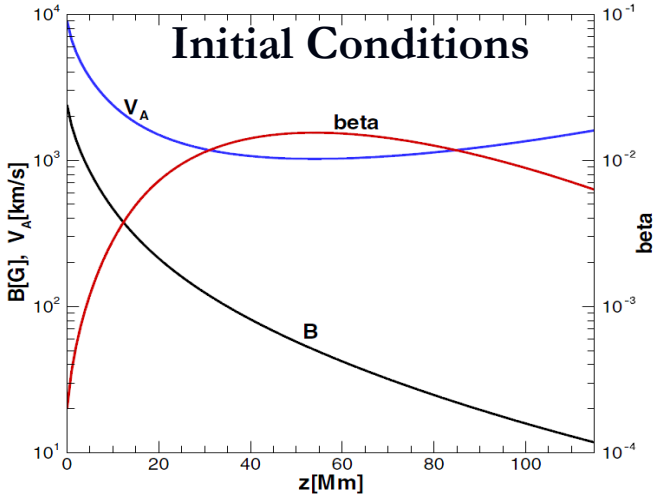

Figure 2. Typical configurations of the magnetic field strength B, the Alfvén speed V_A, and the plasma β along a vertical line through the computation volume.

Driven by time-sequence data of vector magnetgrams

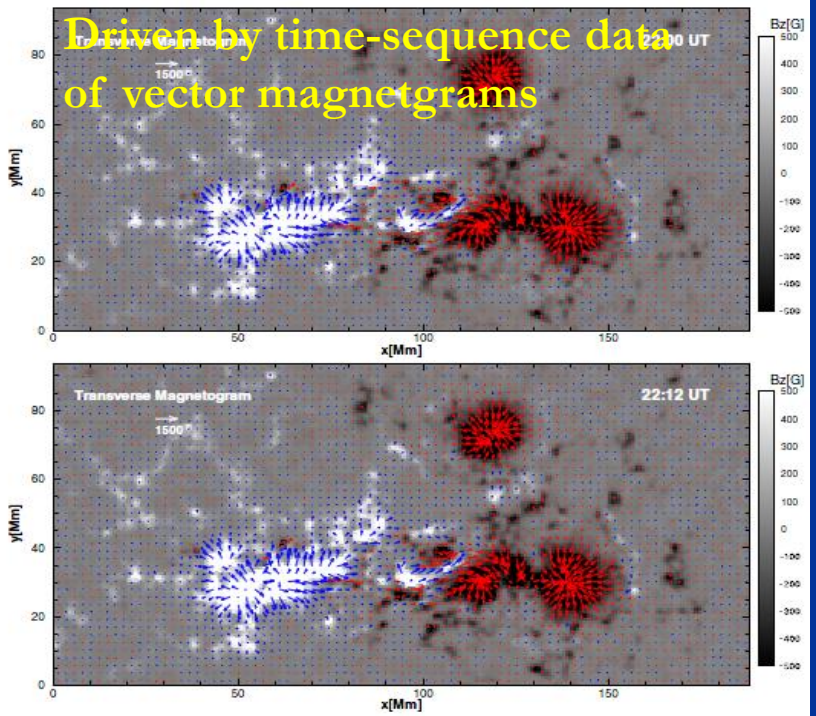

Adaptive Grid

Highest resolution match the magnetogram (e.g., 0.5 arcsec for HMI data); coarsest resolution ~4 arcsec

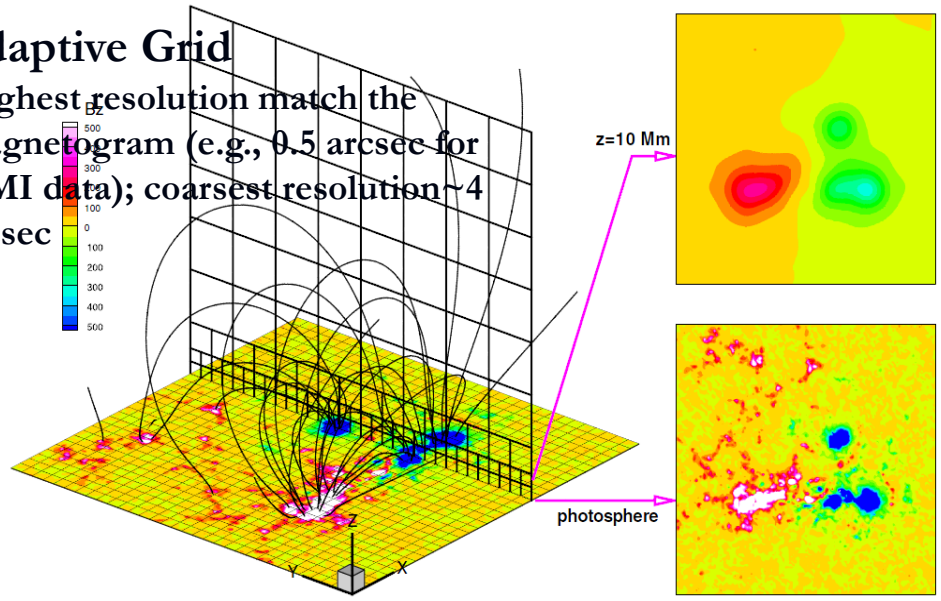

Formation and Eruption of a Sigmoid in AR 11283

- MHD simulation of the eruption process
  - **Full 3D time-dependent MHD model with solar gravity**
  - **Initiated by the NLFFF solutions**; residual Lorentz force as perturbation of the unstable system.
  - No explicit resistivity included, reconnection allowed by numerical diffusion of thin current sheet.
  - Sufficient kinematic viscosity for numerical stability (may reduce the eruption speed)
  - Modeling box: a sub-volume from the NLFFF box; size of $224 \times 256 \times 256$ arcsec^3 with the eruption region at the center of the box.
  - **Adaptive grid: highest resolution ~0.5 arcsec in the sunspot region and coarsest resolution ~4arcsec near the side BCs.**
  - Fixed BCs on the bottom & non-reflecting BCs for numerical boundaries.

Formation and Eruption of a Sigmoid in AR 11283 （ApJL, 2013， 771:L30）

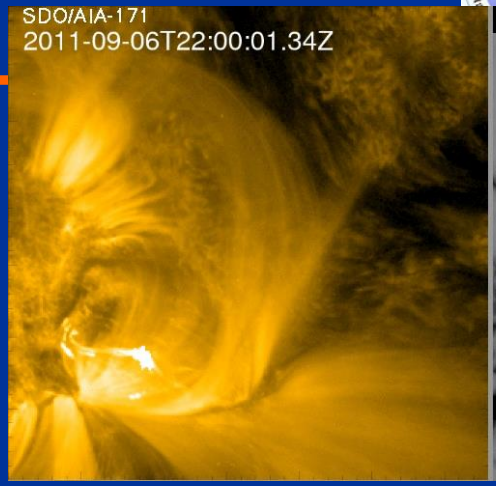

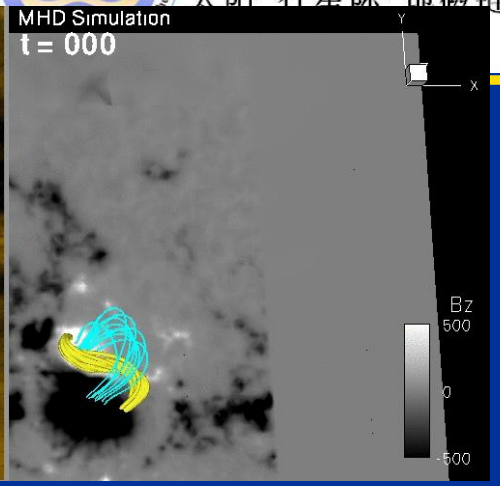

■ MHD simulation

➢ Perfect resemblance of the simulation with AIA observations!

➢ Simulation confirms the eruption mechanism: overlying closed flux (the white lines) reconnected and opened, followed by the rapid rising of the sigmoidal flux rope

➢ Slipping movement of the flux rope footpoint can be both seen in the observation and simulation (slip-running reconnection, Aulanier et al. 2006).

➢The south leg becomes faint because the field twist is weaker and the plasma can easily flow back down by gravity

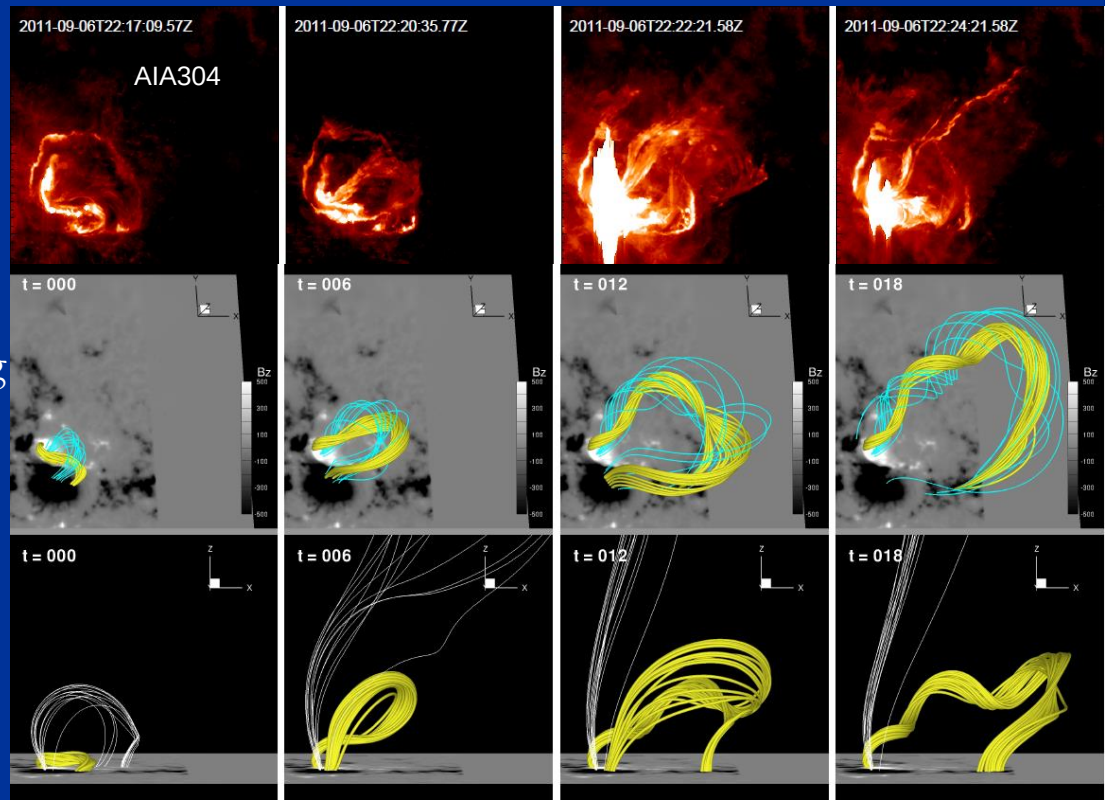

Related Papers

SIGMA Weather Group
太阳-行星际-地磁链
天气团队

[1] Jiang, C. W., Wu, S. T., Feng, X. S., and Hu, Q. (2013), Formation and Eruption of a AR Sigmoid: NLFFF Modeling and Data-Driven MHD Simulation, ApJ, to be Submitted.

[2] Jiang, C. W., Feng, X. S., Wu, S. T., and Hu, Q. (2013), MHD Simulation of a Sigmoid Eruption of Active Region 11283, ApJL, 771:L30.

[3] Jiang, C. W. and Feng, X. S. (2013), Preprocess the Photospheric Vector Magnetograms for NLFFF Extrapolation using a Potential Field Model and a Optimization Method, Solar Physics, In press.

[4] Jiang, C. W. and Feng, X. S. (2013), Extrapolation of the Solar Coronal Magnetic Field from SDO/HMI Magnetogram By A CESE–MHD–NLFFF Code, ApJ, 769, 144.

[5] Jiang, C. W., Feng, X. S., S. T. Wu, and Hu, Q. (2012), Study of the Three-dimensional Coronal Magnetic Field of Active Region 11117 around the Time of a Confined Flare Using a Data-Driven CESE-MHD Model, ApJ, 759, 85.

[6] Jiang, C. W. and Feng, X. S. (2012), A New Implementation Of The Magnetohydrodynamics-Relaxation Method For Nonlinear Force-Free Field Extrapolation In The Solar Corona, ApJ, 749, 135.

[7] Jiang, C. W., Feng, X. S., and Xiang, C. Q. (2012) A New Code For Nonlinear Force-Free Field Extrapolation Of The Global Corona, ApJ, 755, 62.

[8] Jiang, C. W. and Feng, X. S. (2012), A Unified and Very Fast Way for Computing the Global Potential and Linear Force-Free Fields, Solar Physics, 281(2), 621.

IV: Future Avenue

SIGMA Weather Group
太阳-行星际-地磁链
天气团队

- **Further improve and perfect our continuously data-driven time-dependent solar wind background and active region modeling suite**

- **Use the time-dependent numerical results for active regions as initiation to drive the CME from the Sun to Earth**

- **Speed up the model's calculation and data visualization study**

Thanks & Merci